# Quantifying and Reducing Variability in Spark Assisted Chemical Engraving Gravity Feed Drilling in Glass

Andrew Robert Thomas Morrison

A Thesis

in

the Department

of

Mechanical and Industrial Engineering

Presented in partial fulfillment of the requirements
for the Degree of Master of Applied Science (Mechanical Engineering) at
Concordia University
Montreal, Quebec, Canada
December 2009

*Your file Votre référence*
*ISBN:* 978-0-494-67240-2
*Our file Notre référence*
*ISBN:* 978-0-494-67240-2

# Abstract

Quantifying and Reducing Variability in Spark Assisted Chemical Engraving in Glass.

***Andrew Robert Thomas Morrison***

This thesis presents a study of the variability in spark assisted chemical engraving (SACE) gravity feed drilling in glass. SACE gravity feed drilling is a novel micromachining technology for use on non-conducting materials that has yet to move beyond academic investigation. However, SACE is a promising technology. It can be used to create high quality structures, at low cost, using a machine that could be installed into any laboratory. One problem SACE faces is it has issues with reproducibility. This is why the variability of the process is studied here.

The goal of this thesis is to quantify and reduce the variability in SACE gravity feed drilling. This goal is accomplished through three steps. First, the process is modeled to provide an efficient way to quantify variability. Two new stochastic models are presented that relate the depth evolution of SACE gravity feed drilling to the voltage. Statistical tests are used to validate the models. Second, experimental studies of the variability of the depth evolution are discussed. The effect on the variability of having poorly regulated bulk electrolyte temperature and level is studied. Finally, experimental results from two feedback controllers that are capable of reducing the variability in SACE gravity feed drilling are discussed. The results from these controllers are compared with the predictions of one of the models developed.

# Table of Contents

# Table of contents: detailed

## List of Figures

## List of Tables

## Table of Symbols

| Symbols | Meaning |
|---|---|
| $a$ | Gain selecting parameter |
| $c_v$ | Coefficient of Variation |
| $d[n]$ | Bernoulli random process |
| $f_d[n]$ | Probability of d being one |
| $R$ | Normal random variable |
| $s$ | Sample standard deviation |
| $U_m$ | Machining voltage |
| $U_{m,Nominal}$ | Nominal machining voltage for first controller |
| $U_{max}$ | Starting machining volt |
| $U_{min}$ | Minimum machining voltage reached in second controller |
| $v$ | Average speed of drilling |
| $v_0$ | Initial average speed of drilling |
| $v_{lim}$ | Limiting average speed of drilling |
| $X[n]$ | Normal random process |
| $Y[n]$ | Total change each time step, random process |
| $\langle z \rangle$ | Mean of modeled depth |
| $z$ | Depth of a hole drilled, or of a sample of a model. |
| $z_i$ | Depth of the ith hole drilled |
| $\bar{z}_t$ | True mean of the process |
| $\delta$ | Characteristic depth |
| $\kappa$ | Normalized Heat Power |
| $\lambda$ | Rate parameter of Poisson random variable |
| $\lambda_{dec}$ | Parameter that indicates how fast $U_m$ goes from $U_{max}$ to $U_{min}$ |
| $\mu$ | Mean distance of each discrete jump in models |
| $\sigma$ | Variance of each discrete jump in models |
| $\sigma_Y$ | Variance of Y (see above entry for Y) |

# 1 Introduction

## 1.1 The Spark Assisted Chemical Engraving Process

Spark Assisted Chemical Engraving (SACE) is one among a number of micro-machining technologies. This unconventional technology, also known in the literature under the names Electro Chemical Discharge Machining (ECDM) and Electro Chemical Spark Machining (ECSM), is based on electro-chemical discharge phenomena [1, 2]. Two electrodes of very different surfaces are dipped into an electrolytic solution, typically 30%wt NaOH (figure 1-1). The electrode with the smaller surface, which is used as the tool (termed in the following the "tool electrode"), can be either polarised as a cathode or an anode. A gas film will form around it beyond a critical voltage (this value is a function of the electrode geometry, and electrolyte composition and concentration [3]) resulting in intermittent electrical discharges between the electrode and electrolyte through this gas film. If the work piece is brought close to the tool-electrode, glass and other materials can be machined.

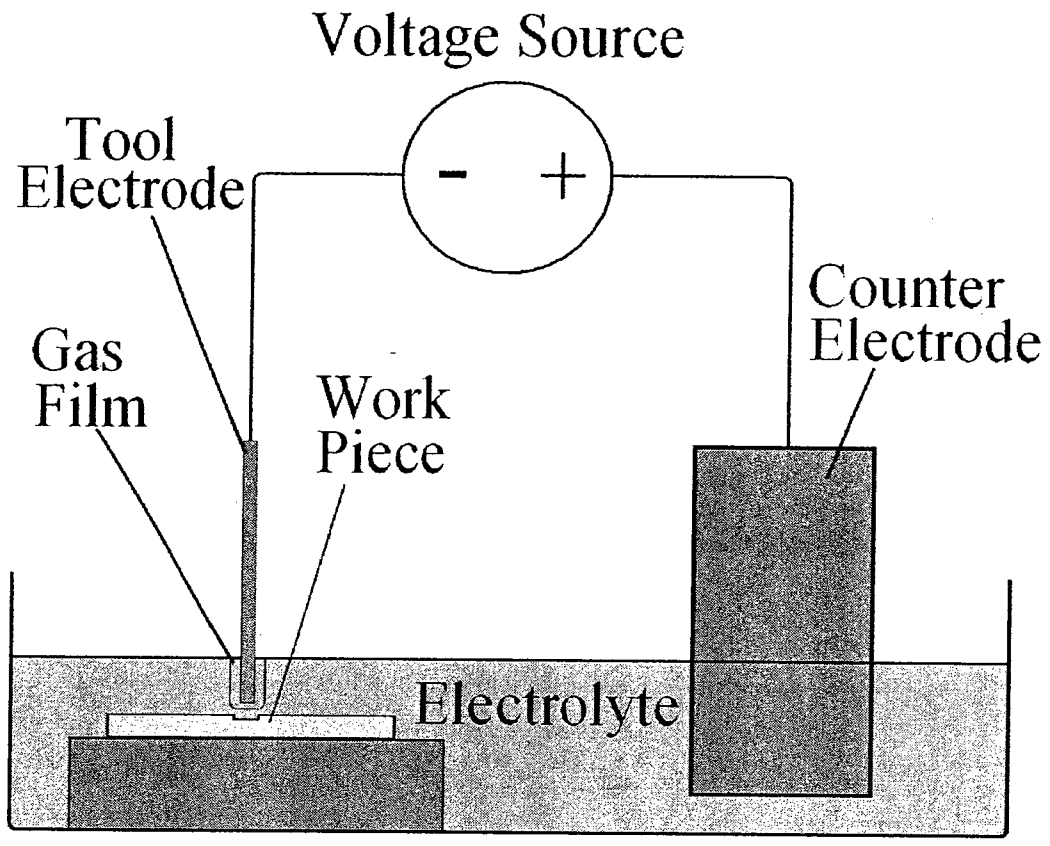


*Figure 1-1: Basic SACE set-up during machining. The tool electrode has a gas film formed around the portion submerged which electrochemical discharges are occurring across. The gas film and discharges are occurring because there is a DC voltage across the two electrodes higher than the critical value. The work piece is being machined due to the presence of discharge activity.*

SACE is a versatile machining process. It can be used to drill microholes, as well as to machine 2D or even 3D structures [1, 4]. Currently the SACE process is solely a subject of academic study. There have been no industrial applications, although some work has been done to adapt the process to this end [5]. In particular, SACE has been used to fabricate prototype units for micro-electromechanical systems and microfluidic devices in laboratory settings [6-8].

## 1.2 Literature Review

The focus of this research is primarily on furthering the knowledge of, and improving upon, micro-hole drilling in glass using SACE. Therefore the state of the art of SACE micro-hole drilling will be discussed here. After discussing the primary methods of micro-hole drilling, recently reported methods of improving SACE drilling, and their limitation, will be pointed out.

### 1.2.1 Constant Velocity Drilling

In constant velocity drilling, after a machining voltage is applied across the tool and counter electrodes, the tool is moved into the work piece at a constant rate. This rate cannot exceed the limiting speed of the process and in general depends on the machining voltage used [9].

### 1.2.2 Gravity Feed Drilling

Gravity feed drilling is the most common approach for micro-hole drilling with SACE [2]. In gravity feed drilling, the tool is fed into the work piece with a constant force. A common method to generate a constant force is to place a known weight on top of the tool, and allow gravity to supply the force that feeds the tool into the work piece [3] (figure 1-2).

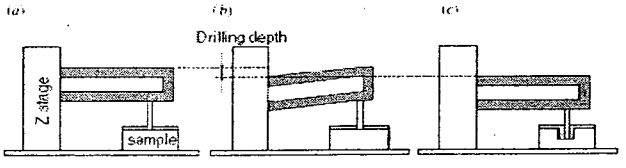


*Figure 1-2: Steps of gravity feed drilling: a) Tool starts in contact with glass surface b) The flexible structure to which the tool is attached is moved down, placing the weight of the structure on the tool. A machining voltage is applied, and machining begins. c) The desired depth is reached and the voltage is switched off* [3].

One advantage of gravity feed drilling over constant velocity drilling is that the depth of the hole can be known at all times because in gravity feed drilling the tool electrode maintains contact with the bottom of the hole. Tool wear is not an important issue as it is known to be very low (7μm in stainless steel after machining for 3 minutes) [1, 10].

There are two regimes known to govern the behaviour of SACE gravity feed drilling [3]: the so-called *discharge regime*, at depths lower than 100 -200μm, and the *hydrodynamic regime* at depths higher than 300 μm. There is also a transition between these two regimes. At shallow depths, in the discharge regime, machining is very fast, reaching speeds up to 100 μm/s. In the hydrodynamic regime machining is much slower, eventually reaching a limiting speed of only a few micrometers per second [3, 11].

#### *1.2.2.1 Speed of Gravity Feed Drilling*

The initial speed, in the discharge regime, is limited by the diffusion inside the work piece of the heat generated by the discharges, and so increases with voltage and thermal conductivity of sample [3, 12]. If machining is assumed to occur when the glass reaches a certain temperature, the initial drilling speed can be estimated accurately [11]. In the hydrodynamic regime speed is limited by the drag on the tool imposed by movement into the softened glass. The final limiting speed in the hydrodynamic regime can be calculated by considering the force of drag on the tool, and the force applied to the tool [11].The limiting speed increases with the applied force, although the effect is not as strong as voltage [3, 11].

The machining speed is also affected by parameters other than machining voltage and force. The speed of SACE drilling is known to increase with the bulk temperature of the

electrolyte [13]. The electrolyte level affects the inter-electrode resistance, a higher level leading to a lower resistance. Lower inter-electrode resistances result in much faster drilling, but the effect lessens with higher voltage [3]. Tool shape affects the speed; using a pointed tool, rather than a flat bottomed tool produces higher speeds [3]. Also, the choice of electrolyte has an effect on speed. Using alkaline electrolyte, instead of acid, increases speed. Within alkaline electrolytes, using KOH instead of NaOH increases speed [14].

A model for gravity feed drilling was proposed in [11] for the mean depth evolution of the process (see section 2.2 for further details). That the model only deals with the mean value of depth evolution is important because the SACE process is stochastic, even under well controlled circumstance [2, 3, 5, 11, 15-18]. Variability in the depth evolution can be seen in figure 1-3 showing the depth evolution of two holes drilled under identical conditions. Also of importance in figure 1-3 is how the depth follows a staircase-like evolution, with short periods of very high speed interspersed with periods of very slow drilling.

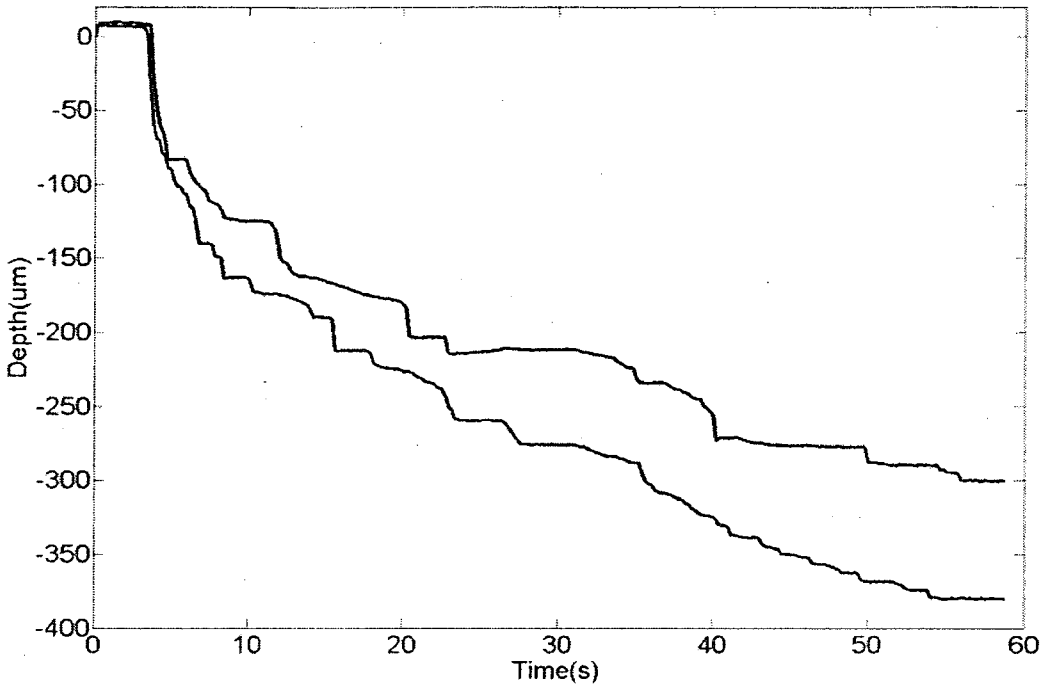


*Figure 1-3: Two typical SACE gravity feed drilling depth evolutions. Both evolutions are drilled under the same conditions. Note both the staircase evolution, as well as the difference between the two evolutions.*

The first ten holes drilled in a set have been known to be generally different than the following ones, which tend to cluster around some mean [3]. However, even after the ten holes have been drilled the process still presents significant variability. For example, in a set of holes which is 275 μm deep, there can be 15 seconds in standard deviation for the drilling time, if a machining voltage of 28V is used (mean machining time is 55s) [16]. Similarly for a machining voltage of 37 V the standard deviation in drilling time is 5 s, with a mean drilling time of 10 s [16].

### *1.2.2.2 Hole Properties*

The process is not only variable in the depth evolution but also in the shape of the hole. For example, for drilling at higher voltages the variation in hole diameter can be up to 100μm for a hole of mean diameter of 540 μm [16].

High quality holes can be achieved with SACE gravity feed drilling, but low quality holes are also possible. The quality of SACE gravity feed drilled micro-holes can be separated into four categories [16] (figure 1-4).

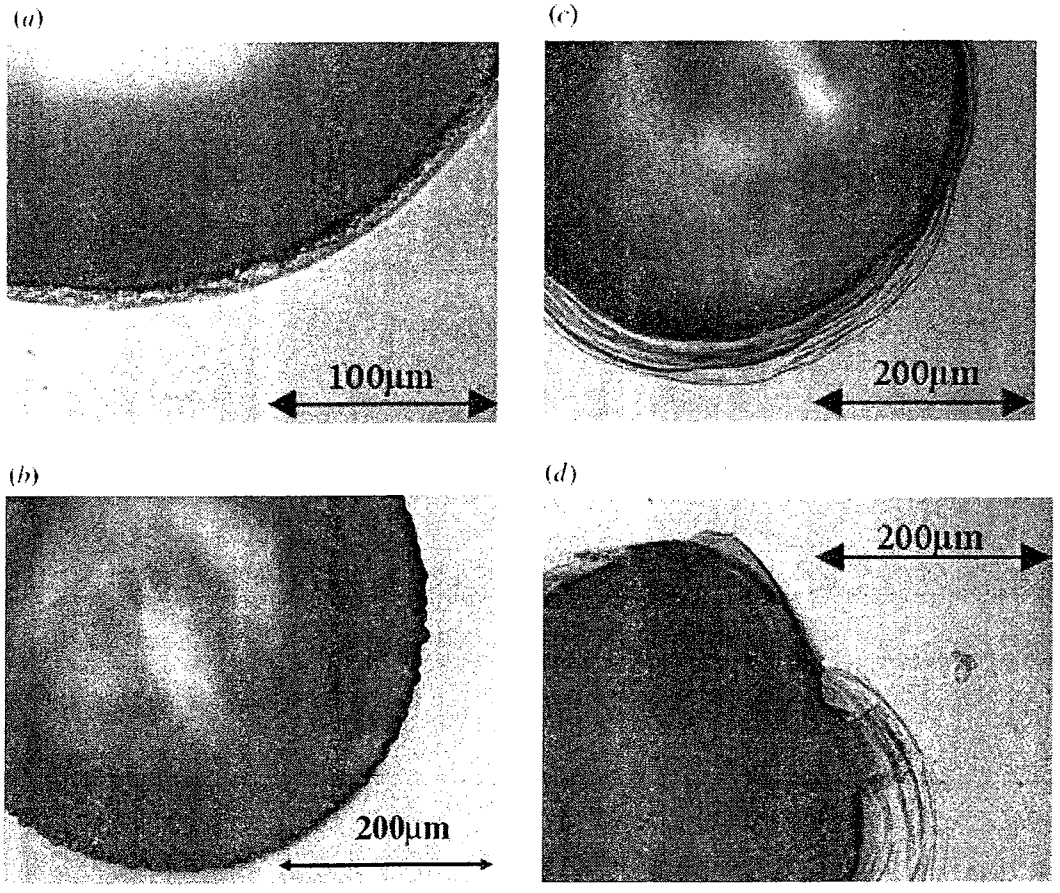


*Figure 1-4: The four categories of micro-hole quality. a: Well-defined cylindrical contours with smooth surface, b: Jagged outline contours, c: Hole with a heat-affected zone, d: Hole with thermal cracks* [16]. *The conditions that produce each of these types of holes can be seen in Figure 1-5.*

In the standard gravity feed drilling two of the most important factors are the machining voltage and the depth drilled. The higher the voltage is, the lower the quality is. There is a similar effect with the drilled depth; deeper holes lead to poorer quality. These two relationships are expressed graphically in figure 1-5 [16]. However, no variability of quality within these general zones has been quantified so far.

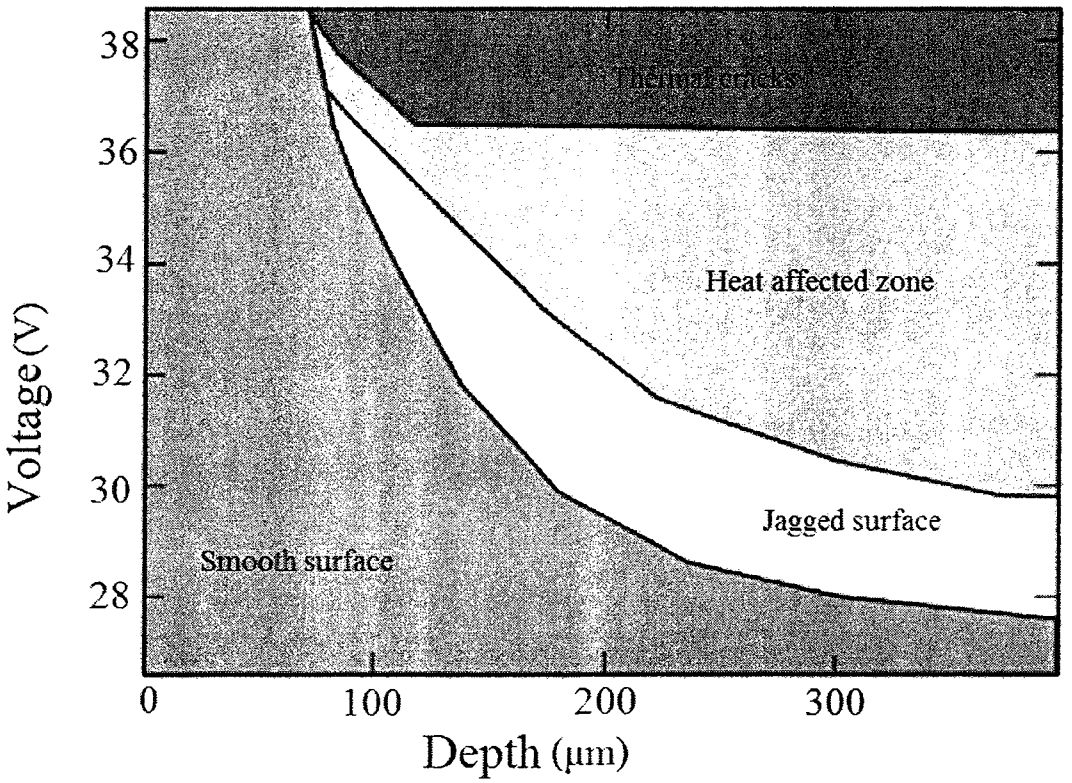


*Figure 1-5: The zones of quality for combination of depth drilled and machining voltage* [16]. *The four zones in the graph(smooth surface, jagged surface, heat affected zone, and thermal cracks) correspond to what is shown in Figure 1-4.*

### 1.2.3 Tool Electrode Motions

Imposed motions of the tool electrode can affect the machining rate as well as the quality of holes. Use of vertical tool electrode vibration with an appropriately chosen frequency and amplitude increase the speed of drilling [19]. In [20] tool rotation is seen to increase drilling speed. However, in [21] tool rotation is seen to decrease drilling speed, while also decreasing the entrance diameter of the microholes. The entrance diameter is decreased down to a minimum at a speed of 1500 rpm; beyond this the entrance diameter grows. Also, in a modification of constant velocity drilling, departing from the constant feed rate allows holes to have more complicated shapes than merely cylinders (e.g. holes with an "hour glass" profile) [7].

### 1.2.4 Voltage Pulses

Voltage pulses have been seen to affect the shape and roughness of drilled holes. Keeping the time a voltage pulse is kept on constant to allow the gas film enough time to build up and varying the time the voltage is off, a decrease in the off time has been shown to decrease the entrance taper on machined holes. An off time of 1ms was found to be an ideal value since higher off times also lead to longer drilling times [21]. The addition of pulses is seen to increase the length and variability of machining time. However, the addition of an offset voltage during the "off" period of the voltage pulses reduces this effect [22]. Using voltages pulses also causes machined holes to have smoother surfaces. The surface smoothness increases with both the frequency of the pulses and their duty cycle. Unfortunately, it is a quality for speed trade off such like what exists when using DC voltage.[23] It is unfortunately not clear whether this quality vs. speed trade off is better than the one made with DC voltage as no proper comparison has been made.

### 1.2.5 Miscellaneous Modifications

There are several other modifications to the SACE process that have been reported, but do not fit into a single category. For example, applying ultrasonic pulses to the electrolyte, while using a tool with an insulated side wall and pulsed machining voltage, was found to improve the speed of drilling and maintain a good quality hole [24]. In another study [25], a load cell was installed under the work piece and the tool was backed off if the force ever became larger than a set value. The results from [25] appear good, although it is hard to tell precisely because there is no comparison with a more standard approach. Additionally, the polarity of the tool electrode is known to affect the shape of holes drilled [8, 13, 26]. Finally, adding abrasive material to the electrolyte can improve the surface quality [27].

### 1.2.6 Feedback machining

Currently no common method of feedback control is used on the SACE process. In fact, no experiments had even been done with feedback till recently [18]. Feedback control is regarded as the solution to many of SACE's problems [1]. Before such a controller can be created a sensor signal must be identified as containing information about the quality of the hole. So far, only the current signal has been examined in detail in this regard. The current signal was found to be lacking in a few regards. The current signal contains high bandwidth information about the sparks crossing the gas film gap, although it is potentially difficult to process this in real time. Additionally, no correlation was found with the material removal rate and the rate of discharge events. On the other hand, the low frequency portion of the current signal can be used to determine whether or not machining is occurring, in a "yes" or "no" manner [17].

### 1.2.7 Comparison

Table 1-1 briefly shows the different ways that variation is reported for SACE drilling.

| Source | Description of Study | Method Variation Reported in |
|---|---|---|
| M. Jalali *et al* [11] | Developing SACE drilling model | Standard deviation of the parameters the model is fit. |
| Z. Zheng et al [22] | Experimenting with Pulsed Voltage SACE Drilling. | The standard deviation, over 30 holes drilled, of the time taken to reach a depth of 450 µm, at a machining voltage of 40 V. |
| P. Maillard et al [16] | Characterizing the geometrical characteristics of SACE drilled holes. | The standard deviation, over 40 holes after discounting the first 10, of time taken to reach the depths of 75, 175, and 275 µm, at machining voltages of 28, 30, 33, and 37 V. |

*Table 1-1: Comparison between different drilling strategies.*

The main conclusion from this table is that existing studies in SACE do not present results about variation in a manner that can be consistently compared to each other. This makes it difficult to evaluate whether or not a reported technique for SACE microhole drilling is worth pursuing or not.

## 1.3 Objectives

The overall objective of this thesis is to quantify and reduce the variability in the SACE gravity feed drilling process. More specifically the variability of the depth evolution will be studied. Depth is used because it is a readily available signal in gravity feed drilling

and has therefore a great potential for practical applications. The overall goal of this thesis is met by the development of:

1. **A stochastic model of SACE gravity feed drilling which can quantify the variability.** The idea is to provide a tool to help quantify how variable a given SACE experiment is. The model developed must be simple, while still agreeing statistically with experiments. As such, it will be made to agree with the state of the art mean field model in its mean value, and agree with experiments in its variation. Such a model is presented in chapter 2.
2. **Measurements of the experimental variation under various conditions.** Chapter 3 presents experimental results quantifying the variability in the SACE process. In addition to results from the standard SACE gravity feed experiment, results using better control of electrolyte level or bulk temperature, and tool vibration are examined. Some combinations of these modifications are also investigated.
3. **Methods to reduce variation in SACE gravity feed drilling.** Some open loop strategies of reducing variation are seen in chapter 3. However, more important in this regard is chapter 4, where closed loop controllers are demonstrated to be able to reduce the standard variation.

## 1.4 Contributions

The main contributions of this thesis are:

1. **Models:** The models are accurate to a statistically significant level for time dependent machining voltage in terms of expected value and variance. This is an

improvement over the state of the art model, which only handled constant voltage and expected value. The model is shown to accurately predict an aspect of gravity feed drilling that it was not designed to, namely, that the process always reaches a steady state in coefficient of variation. The model provides an efficient means of quantifying variability in gravity feed depth evolutions.

2. **Variation Experiments:** Variability of gravity feed drilling is quantified in a systematic manner using statistical tools for the first time. From this quantification, information about the sensitivity of the gravity feed drilling process to bulk temperature and electrolyte level has been determined. Additionally, it is demonstrated that regulation of the bulk temperature and electrolyte level lead to a largely reduced variability.
3. **Feedback Control:** Two feedback controllers, which feed depth into machining voltage, are experimentally shown to have a great impact on the variation of the SACE gravity feed drilling process. This impact is more significant than regulation of bulk temperature and electrolyte level. Combining regulation of electrolyte bulk temperature and level with one of the controllers is seen to decrease the variability further.

# 2 Modeling Gravity Feed Drilling

A model of the time evolution of the drilling depth during SACE gravity feed drilling is presented in this chapter. The objective of the model is to quantify the variability of the depth evolution in SACE gravity feed drilling process. Therefore, the model presented in this chapter extends the state of the art model.

Two stochastic models are presented in this chapter, both inspired by the staircase depth evolutions observed in SACE gravity feed drilling. They are developed taking care to keep them as simple as possible to increase their practically. The first model is a discrete time model, while the second is a continuous time model. The basic assumption of both models is that the depth evolution of the process is the ideal version of the staircase evolution, with perfectly flat horizontal portions, and perfectly vertical random jumps between them. In both models, the random jumps are assumed to be normal, independent and identically distributed. The rate of the jumps, however, is assumed to depend on time, in the discrete time model, and on depth in the continuous time model. Both models are first developed for constant machining voltages before being extended to time dependent machining voltages. Their expected values are compared to the mean field model, and their variances are compared to experimental data. Validation is done by statistic hypothesis testing between the means and variances of the models and experiment. The derived models allow a compact description of the variability observed during SACE drilling. Further, it is shown that the coefficient of variation of the drilling depth evolution reaches a steady state value and can therefore be used as a parameter to characterize the process variability globally. This parameter appears to be a promising candidate to compare depth evolutions done under different conditions efficiently, and

therefore, to be used as a quantitative quality indicator of strategies aimed at reducing variability.

## 2.1 Introduction

As previously mentioned, two models of SACE gravity feed drilling are presented in this chapter. The models are created to provide a tool in describing the variability of the SACE gravity feed drilling process. The models will describe the relationship between the applied machining voltage and the depth evolution.

There is a large amount of variability in depth evolutions of gravity feed drilling. This variability is present even when the process variables are well controlled. The model presented here does not attempt to explain exactly where this variability comes from. Instead, the model is stochastic, treating the gravity feed drilling process as an innately random process. This approach provides some information about the variability seen from hole to hole, without explicitly predicting the exact depth evolution a given hole will have.

### 2.1.1 Statistics

To characterise the stochastic nature of the drilling process, various statistics are used. They are defined and explained here for reference.

The depth sample mean for n drilled holes is

$$\bar{z}(t) = \frac{1}{n}\sum_{1}^{n} z_i(t), \tag{2.1}$$

where $z_i(t)$ is the depth of the *ith* hole at time t. The depth sample standard deviation is

$$s(t) = \left(\frac{1}{n-1}\sum_1^n \left(z_i(t) - \bar{z}(t)\right)^2\right)^{1/2}, \tag{2.2}$$

and the coefficient of variation is

$$c_v(t) = {}^{s(t)}\Big/_{\bar{z}(t)}. \tag{2.3}$$

The coefficient of variation is a useful statistic for comparing the variation of two distributions that have significantly different means.

Three test statistics are used in this chapter for statistical hypothesis testing: the one-sample T-Statistic, the two-sample T-Statistic, and the F-Statistic. Using each of these test statistics is done in the same way. If the test statistic is in a certain range, the critical range, it is concluded that there is enough evidence to reject a hypothesis. Alternately, if the value of the statistic is outside that range, it is concluded that there is not enough evidence to reject the hypothesis (note this is different than the hypothesis being true). The range is determined by first selecting the level of significance α. Through this work we use α =0.05. The level of significance is the probability of incorrectly rejecting the hypothesis. Using α and the proper table from [28], the critical value for the statistic is determined. All three statistics are used here to test null hypothesises of the form

$$H_0: q_1 = q_2 \tag{2.4}$$

against alternate hypothesises of the form

$$H_1: q_1 \neq q_2, \tag{2.5}$$

where $q_1$ and $q_2$ are the two quantities that are tested with the statistic. Table 2-1 shows what hypothesis each test statistic tests, how to calculate its value, and what the critical range for it is.

| Test Statistic | $q_1$ | $q_2$ | Equation | Critical Range |
|---|---|---|---|---|
| One-Sample T | $\bar{z}_t(t)$ | $\langle z_h(t)\rangle$ | $T_1(t) = \frac{\bar{z}(t) - \langle z_h(t)\rangle}{s(t)/n}$ | $\lvert T_1(t)\rvert > t(\alpha, n)$ |
| Two-Sample T | $\bar{z}_t(t)$ | $\langle z_h(t)\rangle$ | $T_2(t) = \frac{\bar{z}(t) - \bar{z}_h(t)}{\sqrt{\frac{s(t)}{n} \frac{s_h(t)}{n_h}}}$ | $\lvert T_2(t)\rvert > t(\alpha, n, n_h)$ |
| F | ${s_T}^2(t)$ | $s_{h\,T}^2(t)$ | $F(t) = \frac{s^2(t)}{s_h^2(t)}$ | $F(t) > f(\alpha, n, n_h)$ or $F(t) < {}^1/_{f(\alpha, n, n_h)}$ |

*Table 2-1: Test Statistic Properties. In each case, if the value determined by the equation is within the critical range then there is enough evidence to reject the hypothesis that $q_1$ is the same as $q_2$*

The new variables introduced in Table 2-1 are described below:

- $\bar{z}_t(t)$ is the true mean of the process (as opposed to the sample mean from an experiment),
- $\langle z_h(t)\rangle$ is the mean of the hypothesized model.
- $n$ is the number of samples from an experiment, $n_h$ is the number of samples used from the hypothesized model
- $\bar{z}_h(t)$ is the sample mean, and $s_h(t)$ is the sample standard deviation of the hypothesized model.
- t, and f are critical values for the rejection or non-rejection of null hypothesises.
- $s_T(t)$ is the true variance of the process, and $s_{h\,T}^2(t)$ is the variance of the hypothesized model.

### 2.1.2 Probability distributions

Two common types of probability distributions are used in this chapter. Information about them is briefly summarized here.

One of the distributions used is the Bernoulli distribution; a discrete probability distribution that takes two values: one or zero. A sample of a Bernoulli distribution will be one with some probability, and zero with a probability that is the complement of the probability of being one.

The Poisson process is also important to this thesis. A Poisson process is a stochastic process that describes a series of discrete events. The number of events occurring in any one interval is independent of the number of events that occurred in any other interval. The Poisson distribution describes the number of events that occur in a fixed interval. There is no hard limit to the number of events that can occur in a interval, thus samples of the Poisson distribution can be any positive integer or zero. The probability of a sampled value, N, taking on a certain value, k, is given by

$$P(N = k) = \frac{e^{-\lambda t}(\lambda t)^k}{k!}, \tag{2.6}$$

where t and λ are parameters of the distribution[1]. Most commonly, t is interpreted as time, and a sample of a Poisson random variable is interpreted as the number of events which occur over t units of time. In that interpretation λ is the average number of events per unit time. Other possible interpretations could use t as a distance or in a more abstract way, but that is not the case here.

[1] The probability distribution of the interval between two events, a continuous random variable, is given by the exponential distribution.

## 2.2 The Mean Field Model

### 2.2.1 State of the Art Model

The mean field model refers to the work developed in [11], which describes the average of the depth evolutions in gravity feed drilling. This is the current state of the art model of gravity feed drilling. A small part of the derivation, and the model itself, are reproduced here following [11].

The mean field model was obtained by noting that there are two regimes for SACE gravity feed drilling. There is the discharge regime, which occurs at low depths, and the hydrodynamic regime, which occurs at high depths (see chapter 1 for more details). During drilling, the process is assumed to transit smoothly between these two regimes. This smooth transition is represented in terms of the mean field model by assuming that the speed is inversely proportional to the depth drilled. The speed decreases with depth from a certain initial velocity $v_0$ to a final velocity $v_{\lim}$. Both velocities can be related to physical parameters of the system [11]. The rate of speed decrease is assumed to be $\delta$. More specifically, the model starts with the differential equation

$$\begin{cases} {}^{dv}/_{d\langle z\rangle} = -{}^{1}/_{\delta}\,(v(\langle z\rangle) - v_{lim}) \\ \langle \dot{z}\rangle = v(\langle z\rangle) \\ \langle z(0)\rangle = 0 \\ v(0) = v_0 \end{cases} \tag{2.7}$$

The solution to this differential equation is

$$v(z) = (v_0 - v_{\lim})e^{-{}^{\langle z\rangle}/_{\delta}} + v_{lim}. \tag{2.8}$$

This is also a differential equation, the solution to which is

$$\langle z(t)\rangle = \delta ln\left[\frac{v_0}{v_{lim}} e^{\frac{v_{lim}}{\delta}t} - \frac{v_0 - v_{lim}}{v_{lim}}\right]. \quad (2.9)$$

In [11] the parameters $v_0$, $v_{lim}$, and $\delta$ were fitted to experimental data. The values measured in [11] are summarized in table 2-2, although new experimental results for these parameters are used throughout this thesis. It is important to note that the reported variation in the parameters is not primarily due to measurement error, but is mostly due to the variable nature of the depth evolution.

| Machining Voltage | $v_0$ (μm/s) | $v_{lim}$ (μm/s) | δ (μm) |
|---|---|---|---|
| 28 | 31 | 1.7±1.5 | 70±18 |
| 30 | 50 | 1.6±0.8 | 77±7 |
| 33 | 85 | 3.1±0.7 | 87±20 |

*Table 2-2: Parameters found in* [11]. *Drilling was done with a 0.4mm stainless steal cylndrical tool in 30%wt NaOH. Error values are standard deviations of the fitted parameters. No error value was reported for* $v_0$.

There are two main limitations in the mean field model. First, it does not describe any of the variability seen in the process. Second, the mean field model was developed only for constant machining voltages. These two limitations will be overcome by the models presented here.

### 2.2.2 Time Dependent Machining Voltage

The mean field model is extended in this section to time dependent machining voltages.

#### *2.2.2.1 Assumptions*

The following assumptions are made:

1: Equation (2.8) is a differential equation which accurately describes the mean depth machined for time dependent voltages if the parameters are allowed to depend on voltage

2: The only parameter that is allowed to change with voltage is $v_0$, which becomes $v_0(U_m(t))$.

The first assumption means that a change in voltage will cause instantaneous changes in the speed, i.e. transient effects of voltage changes are neglected. The second assumption is motivated by a conclusion from [11], stating that only the parameter $v_0$ depends strongly on voltage, while neither of the other two parameters do. There is increase in v0 over 5 volts of 2.75 times, where as for $\delta$ the increase is 1.25 and for $v_{lim}$ 1.8 times. Additionally, the increase with voltage seen in $\delta$ and $v_{lim}$ is within the error bound reported.

#### *2.2.2.2 Formulation*

Assumptions 1 and 2 imply that Equation (2.8) changes to

$$v(z) = [v_0(U_m(t)) - v_{\lim}]e^{-z/\delta} + v_{lim}, \tag{2.10}$$

where $U_m(t)$ is the time dependent machining voltage. Equation (2.10) is a differential equation that can be solved to get

$$\langle z(t)\rangle = \delta ln\left[\frac{1}{\delta}\int_0^t v_0(U_m(s))exp\left(\frac{v_{lim}}{\delta}(t-s)\right)ds + 1\right]. \tag{2.11}$$

#### *2.2.2.3 Validation*

To test this proposed modification of the mean field model, data from three experiments at constant voltage are first fit by least squares to the model. The experiments consist of

50 holes drilled with a stainless steel tool of diameter 0.4 mm, in a 30%wt. solution of NaOH (For more information on experimental set-up and procedure, see chapter 3). The objective of this step is to determine a value of $v_0$ for each voltage. The values of $v_0$ determined for these voltages can be found in table 2-3. The following values were used for the remaining parameters: $v_{lim} = 3.1$ μm/s and $\delta = 70$ μm.

| Machining Voltage (V) | $v_0$ (μm/s) |
|---|---|
| 29 | 32 |
| 30 | 61 |
| 31 | 240 |

*Table 2-3: Parameters measured from constant voltage experiments. Note: parameters measured here are different from table 2-2 because they are based on two different sets of experiments with differing apparatuses. In particular, the over-flow electrode, as described in 3.2.2.2 is used, which causes faster drilling.*

Figure 2-1, shows a plot of the one-sample T-Statistic comparing the extended mean field model and experimental data. The experiment had a step in machining voltage at 30 seconds from 30 to 31 V. This is way only data after 30 seconds is shown. The examined experiment is representative of other experiments done (including a 29 to 30 V step and a 29 to 31 V step). 30 V is a machining voltage that is interesting for practical purposes, which is why the steps close to it were investigated. As can be seen, except for a short duration soon after the step in machining voltage, there is not enough evidence to reject the hypothesis that the model's prediction is not the same as the mean for the system. The slight incongruity close to the switch is possibly due to transient elements. The agreement with experimental evidence justifies the assumptions made, at least for changes in voltage similar to the tested one.

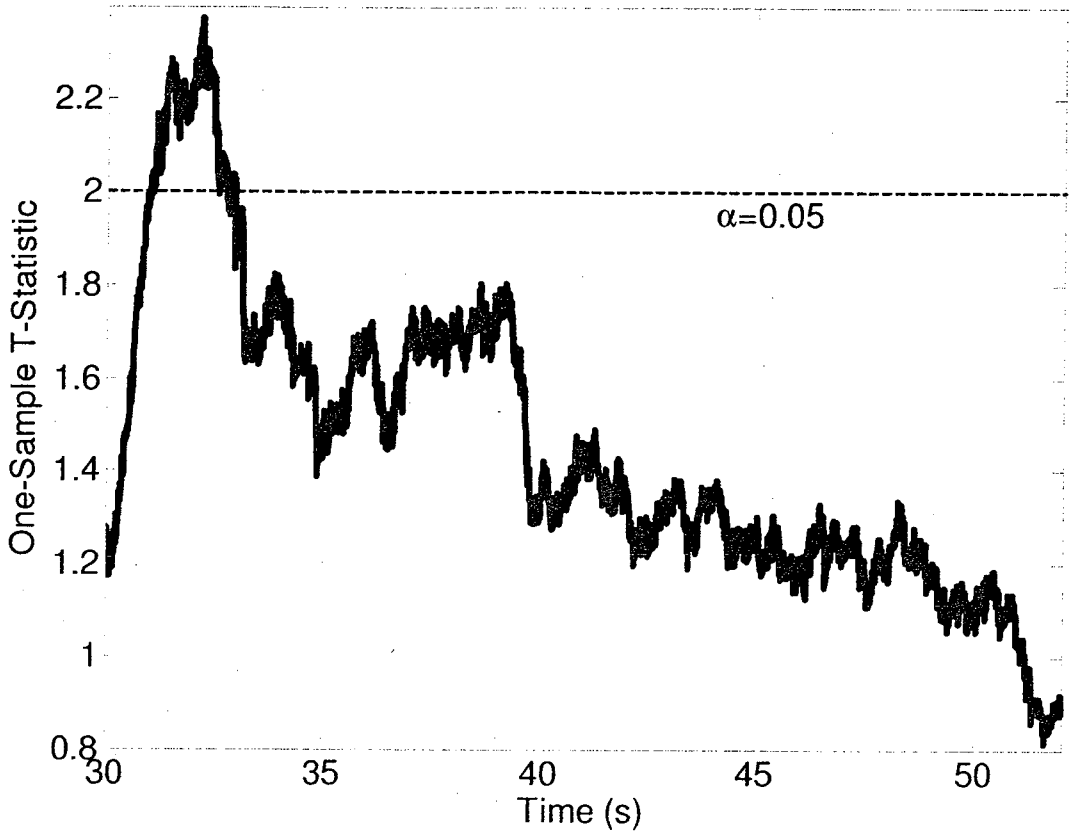


*Figure 2-1: The one-sample T-statistics for the extended mean field model. The experiment had a voltage step from 30 to 31 volts at 30 seconds. The dashed line corresponds to the top of the critical range for α=0.05 (lower line not shown).*

## 2.3 Stochastic model (Constant Voltage)

The form of the stochastic process is inspired by the common pattern seen in SACE gravity feed drilling depth evolutions. The depth of gravity feed drilling often follows a staircase evolution. Explicitly, the evolution can be broken down into regions where very little progress into the work piece is being made, and regions where extremely rapid progress is made. The staircase pattern is not a uniform pattern in the sense that the horizontal and vertical components have variable, and seemingly random, lengths.

Sometimes, the almost horizontal sections can have a significant slope, and there can be gradual transition to a vertical segment. To simplify the model, these less common events will be ignored. A discrete time model and a continuous time model are presented below.

### 2.3.1 Discrete Time Model

#### *2.3.1.1 Assumptions*

The model makes the following assumptions:

1: The process can be described as the ideal staircase evolution. All progress into the work piece is made only in randomly sized discrete jumps, and at all other times no drilling occurs.

2: At most one jump will occur per time step.

3: The probability of a jump at a given step is function only of the current step number.

4: The jump sizes at time steps n=1,...,N are modeled by a stochastic process with identically distributed and independent random normal variables $X_n$ with a mean of $\mu$ (the jump-mean) and a standard deviation of $\sigma$ (the jump-standard-deviation).

5: The size of each jump is independent of when the jump occurs and at what depth it occurs at.

Assumption 1 is the basic assumption of both models. Assumptions 2 to 5 are done to allow a mathematical closed form formulation. Using a normal distribution is an Ansatz, motivated by the central limit theorem.

### 2.3.1.2 Formulation

The step size of the model will be Δt. This is not important in these derivations except when the mean field model is employed.

The model is expressed by,

$$z[0] = 0$$
$$z[n+1] = z[n] + d[n] \cdot X[n] \tag{2.12}$$

where $X[n]$ is a continuous random process, and $d[n]$ is a discrete random process that can take a value of one or zero for each n. These are defined as:

$$X[n] \equiv \begin{array}{c} A\ normal\ stationary\ i.i.d.random\ process \\ with\ mean\ \mu\ and\ standard\ deviation\ \sigma. \end{array} \tag{2.13}$$

$$d[n] \equiv \text{Bernoulli process} \tag{2.14}$$

$$P(d[n] = 1) = f_d(n)$$
$$P(d[n] = 0) = 1 - f_d(n) \tag{2.15}$$

Note that due to assumption 5, X[n] and d[n] are independent. The exact nature of $f_d$will be determined in what follows. The solution to equation (2.12) can be written as the sum

$$z[n] = z[0] + \sum_{i=1}^{n} d[i] \cdot X[i] \tag{2.16}$$

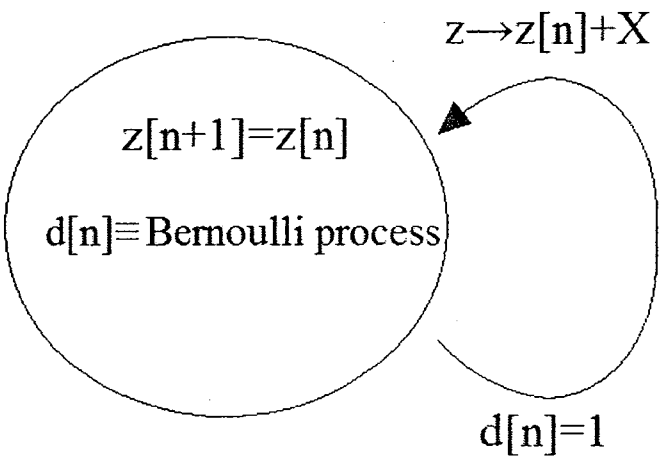


*Figure 2-2: Discrete model state-flow diagram. For each time step d is randomly one or zero. If d is zero z takes the same value as at the previous time step, else if d is one and z takes a value equal to the previous value plus a normal random variable.*

and is depicted in the state flow diagram shown in figure 2-2. Equation (2.16) is a sum of independent mixed random variables. Let

$$Y[n] = d[n] \cdot X[n] \tag{2.17}$$

The mean of $Y[n]$ is computed by exploiting the fact that $d[n]$ and $X[n]$ X[n] are independent of each other. This means that the expected value of their product is the product of their expected values. Using this fact, the mean of $Y[n]$ is

$$\langle Y[n] \rangle = f_d(n) \cdot \mu \,. \tag{2.18}$$

The standard deviation of $Y[n]$, $\sigma^2_{Y[n]}$, can be determined in a similar way. We start with the definition for $\sigma^2_{Y[n]}$:

$$\begin{aligned} \sigma^2_{Y[n]} &= \langle Y[n]^2 \rangle - \langle Y[n] \rangle^2 \\ \sigma^2_{Y[n]} &= \langle d[n]^2 \cdot X[n]^2 \rangle - \langle d[n] \cdot X[n] \rangle^2 \end{aligned} \tag{2.19}$$

Equation (2.19) is expanded as.

$$\sigma^2_{Y[n]} = \langle d[n]^2 \rangle \cdot \langle X[n]^2 \rangle - \langle d[n] \rangle^2 \cdot \langle X[n] \rangle^2 \tag{2.20}$$

Then using,

$$\begin{aligned} \langle X[n]^2 \rangle &= \sigma^2 + \mu^2 \\ \langle X[n] \rangle^2 &= \mu^2 \\ \langle d[n]^2 \rangle &= f_d(n) \\ \langle d[n] \rangle^2 &= f_d(n)^2 \end{aligned} \tag{2.21}$$

into (2.20) yields

$$\sigma^2_Y[n] = f_d(n) \cdot (\sigma^2 + \mu^2) - f_d(n)^2 \cdot \mu^2 \tag{2.22}$$

With the mean of $Y[n]$, found, the mean of $z[n]$, can now be stated using (2.16) and (2.18) as

$$\begin{aligned} \langle z[n] \rangle &= \textstyle\sum_{i=1}^{n} \langle Y[i] \rangle \\ \langle z[n] \rangle &= \mu \textstyle\sum_{i=1}^{n} f_d(i) \end{aligned} \tag{2.23}$$

Similarly, we can write the standard deviation of $z[n]$ using (2.22) and assuming independence of $Y_j$ as

$$\begin{aligned} \sigma^2_Z[n] &= \sqrt{\textstyle\sum_{i=1}^{n} \sigma^2_{Y[i]}} \\ \sigma^2_Z[n] &= \sqrt{\textstyle\sum_{i=1}^{n} (f_d(n) \cdot (\sigma^2 + \mu^2) - f_d(n)^2 \cdot \mu^2)} \end{aligned} \tag{2.24}$$

To make the model's mean match the mean field prediction, the difference between two time samples of (2.23) is considered, and equated to what the difference should be based on the mean field model. The difference between the mean value of the model at two consecutive time steps is

$$\langle z[n] \rangle - \langle z[n-1] \rangle = \mu \textstyle\sum_{i=1}^{n} f_d(i) - \mu \sum_{i=1}^{n-1} f_d(i) \tag{2.25}$$

Equation (2.25) can be solved for $f_d$

$$f_d(n) = \frac{1}{\mu} \cdot [\langle z[n] \rangle - \langle z[n-1] \rangle] \tag{2.26}$$

Equation (2.26) shows that $f_d[n]$ can be determined from the average depth at that time step and the previous depth. To ensure that the same mean as the mean field model is produced, (2.9) (the mean field model) is substituted into (2.26) using $z[n] = z(n \cdot \Delta t)$. It follows that $f_d$ is

$$f_d(n) = \frac{\delta}{\mu}\left[\frac{\left(e^{\frac{v_{lim}}{\delta} n \cdot \Delta t} - 1\right) v_0 + v_{lim}}{\left(e^{\frac{v_{lim}}{\delta}(n-1) \cdot \Delta t} - 1\right) v_0 + v_{lim}}\right] \tag{2.27}$$

From here, the remaining parameters are determined by fitting the equations experimentally. The model is summarized by (2.12)-(2.15), with $f_d$ being given in (2.27). The parameters that remain free to be fitted are $v_0$, $v_{\text{lim}}$, $\delta$, $\mu$, and $\sigma$.

#### *2.3.1.3 Validation*

The mean of the model already matches exactly the existing state of the art model (2.9) by construction. The mean and standard deviation are fit by least squares to experimental data from an experiment done with a constant machining voltage of 30 V. The examined experiment is representative of experiments done at other constant machining voltages (including a 29 and 30 V). 30V is a machining voltage that is interesting for practical purposes, which is why it is used. The plot of the F-statistic vs. time (Figure 2-3) shows there is not enough evidence to reject the hypothesis that the variance of the model and the variance of the experiment are different for most of the machining time. However, for the first 5 seconds there is sufficient evidence to reject the hypothesis that the model's

standard deviation matches with the sample standard deviation. In fact, for the first few seconds of drilling the very large value of the F-Statistic suggests that the model does not even come close to predicting the experiment for those few seconds. All of this indicates that the discrete time model is acceptable for the majority of drilling, with the possible exception of the initial transient of drilling.

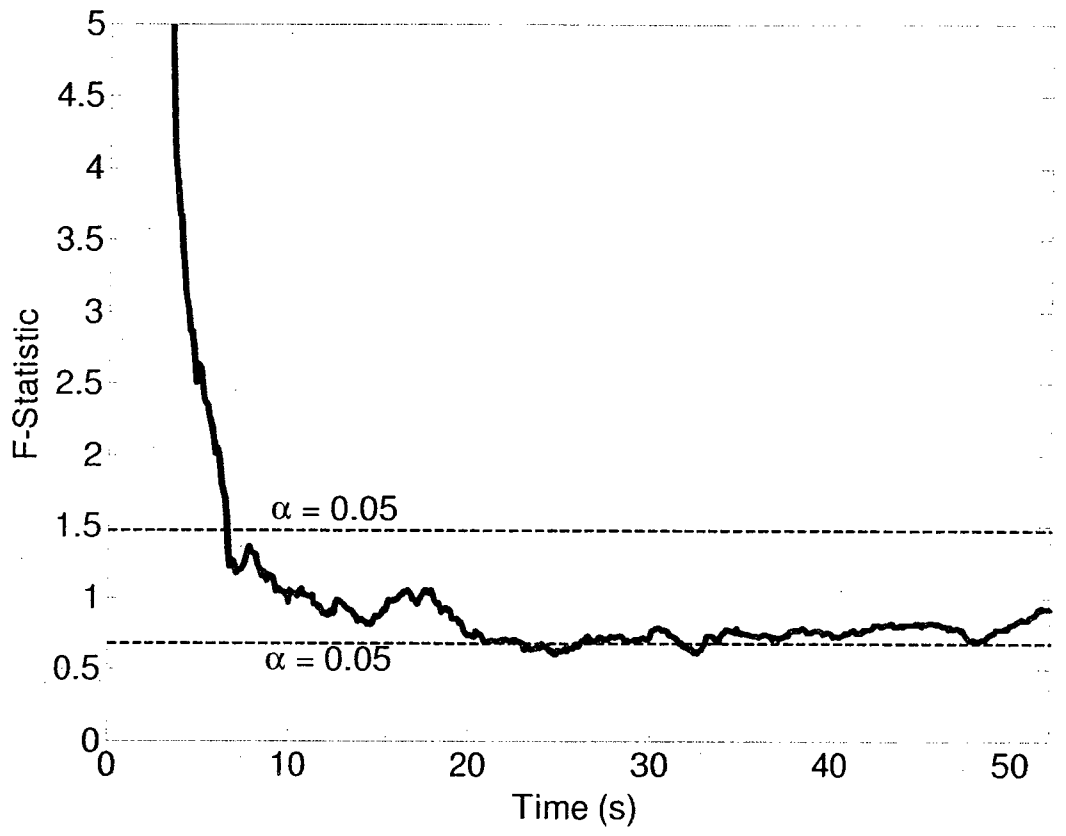


*Figure 2-3: F-Statistic for discrete time model and experimental data from an experiment at 30 V. The dashed lines show the critical range for α=0.05.*

### 2.3.2 Continuous Time Model

#### *2.3.2.1 Assumptions*

The following assumptions are made to derive the model:

1: The process can be described as the ideal staircase evolution. All progress into the work piece is made only in randomly sized discrete jumps, and at all other times no drilling occurs.

2: On the size of each jump:

   A: Each jump is independent off all the others.

   B: The distribution of the size of each jump is normal, with a mean of $\mu$ (the jump-mean) and a standard deviation of $\sigma$ (the jump-standard-deviation).

3: The jumps are a modified Poisson process, with the rate depending on the current depth. The rate of the poison process is $\lambda(z)$ , the jump-rate (note that allowing the rate to be a function of depth is modified from the standard Poison random variable where it is a constant.).

The first assumption is the basic assumption of both stochastic models presented in this chapter. The second is the same as the third assumption in the discrete time model. Assumption 2 is done mainly to avoid complication of the model. However part B is an Ansatz, motivated by the central limit theorem. The third assumption is made in part so that the model can mimic the physical process; the average speed depends on the depth. A modified Poisson process is chosen as the time distribution of the jumps as another Ansatz. A Poisson process is common in nature for processes that occur as discrete events, and it allows the rate of the events to be chosen in a single, depth dependent, parameter, $\lambda(z)$.

#### *2.3.2.2 Formulation*

A model depicted in figure 2-4 can be directly constructed from the assumptions. The model has a single continuous variable, the depth drilled, that is discontinuous at a finite

set of time instants, but is otherwise constant; i.e. is modified only through discrete events. These discrete events occur stochastically as a modified Poisson process, with a rate that is dependent on the depth (assumption 3). Each discrete step updates the continuous variable by adding a random amount to it. This model is similar to models discussed in [29].

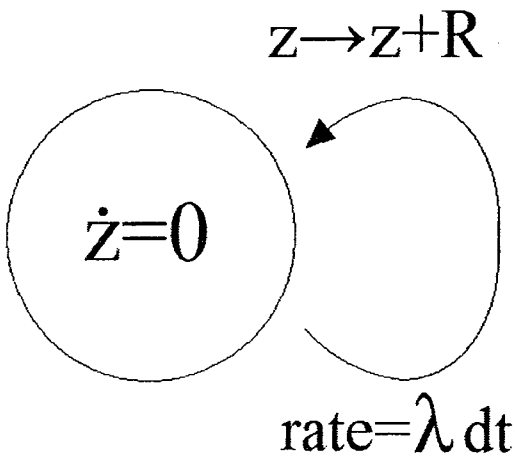


*Figure 2-4: Model form: z is depth, the continuous variable, λ is the rate of the discrete event, and R is a normal random number added to z each time a discrete event occurs.*

The model has three parameters that must be determined: $\lambda(z(t))$, μ, and σ. An equation for $\lambda(z(t))$ will be determined by requiring that the model's expected value follows the mean field model. The expected value of this model is unfortunately not as straightforward to determine analytically as it was in the discrete time model. This difficulty is partly because the rate of random jumps is dependent on the depth. However, it is still possible to work out an answer if an approximation is made. The use of the approximation will be tested when the model is validated.

Consider that $\lambda(z(t))$ is the average number of jumps per second, and that μ is the average amount added to z per jump. It is then clear that the average speed at a certain instant in time is

$$\langle \dot{z}(t) \rangle = \langle \lambda(z(t)) \rangle \cdot \mu \tag{2.28}$$

The brackets are placed around λ because z(t) is a random variable. If the approximation

$$\langle \lambda(z(t)) \rangle \approx \lambda(\langle z(t) \rangle) \tag{2.29}$$

is made, then (2.28) is a differential equation in $\langle z \rangle$, which is similar to (2.8) (which is a differential equation because $v = \dot{z}$). Using this insight, a form of $\lambda(z)$ can be proposed as

$$\lambda(z) = \frac{(v_0 - v_{\lim}) e^{-z/\delta} + v_{lim}}{\mu}. \tag{2.30}$$

With $\lambda(z)$ as defined in (2.30), $\langle z \rangle$ will follow a path close to (2.9). How close depends on how good an approximation (2.29) is.

The model is described by the state flow diagram in figure 2-4, with λ given in (2.30) and $R$ being a normal random variable with mean $\mu$ and standard deviation $\sigma$. There are five free parameters: $v_0$, $v_{\lim}$, $\delta$, $\mu$, and σ. These parameters must be determined by fitting experimental data. The parameters $v_0$, $v_{\lim}$, and $\delta$ are used to fit the mean evolution, while $\mu$, and σ are used to fit the variance. That $\mu$is not used to fit the mean is possible counter-intuitive. However, it becomes more clear when it is seen that substituting (2.30) into (2.28) leads to $\mu$ cancelling out.

#### *2.3.2.3 Simulation*

Simulation of the model is done with a constant time step algorithm. For each time step n, each of which is $\Delta t$ seconds in length, the following is done:

1: Generate the number $\boldsymbol{m}[n]$, a Poisson distributed random number with rate $\lambda = \lambda(z(n \cdot \Delta t))$ using Knuth's algorithm for sampling a Poisson distribution [30].

2: Generate the jump size for the current time step:

$$J[n] = \sum_{i=1}^{\boldsymbol{m}[n]} X_i, \tag{2.31}$$

where the $X_i$ are independent, and identically distributed normal random variables, with mean $\mu$ and standard deviation $\sigma$ (If $\boldsymbol{m}[n] = 0, J[n] = 0$). The next depth value generated is then

$$z\big((n \cdot \Delta t) + 1\big) = z(n \cdot \Delta t) + J[n]. \tag{2.32}$$

#### *2.3.2.4 Discussion*

Figure 2-5, shows some typical results from simulations. An important feature of these graphs is seen in both E and F where the coefficient of variation is shown. Note how the coefficient of variation reaches a steady state value. This behaviour was not a feature that was sought after in developing the model. Experimental results in SACE also show this steady state coefficient of variation, which shows that the model has predictive power beyond that for which it was created. Confirmation of that the coefficient of variation reaches a steady state value in experiments is shown in chapter 3. Notice also that the samples of the model (C and D) qualitatively look like SACE drilling.

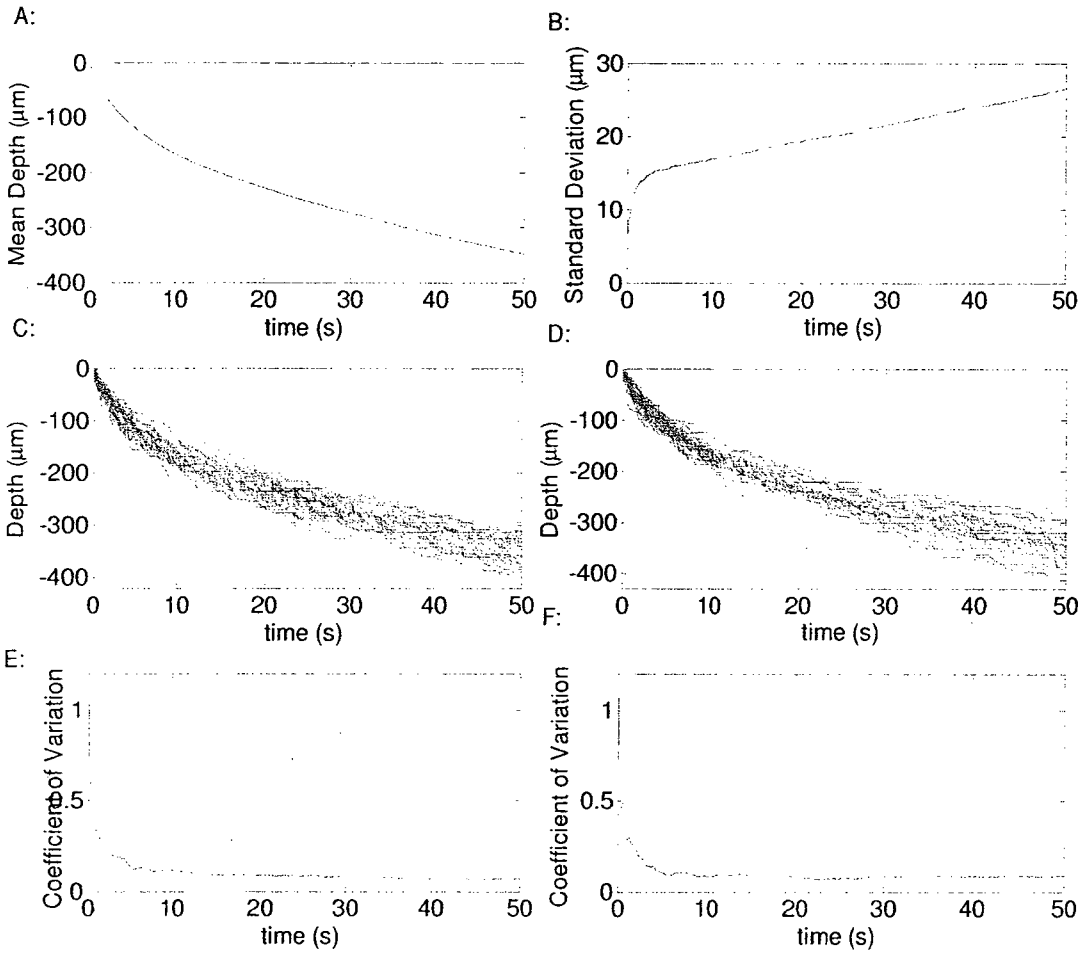


*Figure 2-5 Example plots from model. A: Expected Value, B: Standard deviation, C and D: 50 Sample paths from the model, F and E: the Coefficient of variation for the data from C and D respectively.*

### *2.3.2.5 Validation*

The expected value curve for the model was fit by least squares to the mean field model (2.9) at 30 V in the parameters $v_0$, $v_{\lim}$, and $\delta$. 30 V is used because it is a machining voltage that has particular practical value. The values determined for $v_{\lim}$, and $\delta$ were identical to the parameters used in the mean field model. However the value of $v_0$

determined from the fit was 6 μm/s lower than the value used in the mean field model. The values are presented in table 2-4

| Parameter | $v_0$ | $v_{\text{lim}}$, | $\delta$ |
|---|---|---|---|
| Value | 55 μm/s, | 3.1 μm/s | 70 μm |

*Table 2-4: Values found for parameters by fitting model outlined in 2.3.2.2 to mean field model from 2.2.1 for a machining voltage of 30 V.*

When the fitted parameters are used, the stochastic model agrees very well with experimental data. Given that the model is based on the approximation (2.29), it is not expected that the model should match exactly to (2.9) for the same values of the parameters. Since generation of the same mean evolution is possible with adjusted parameters, the approximation (2.29) has proved to be acceptable.

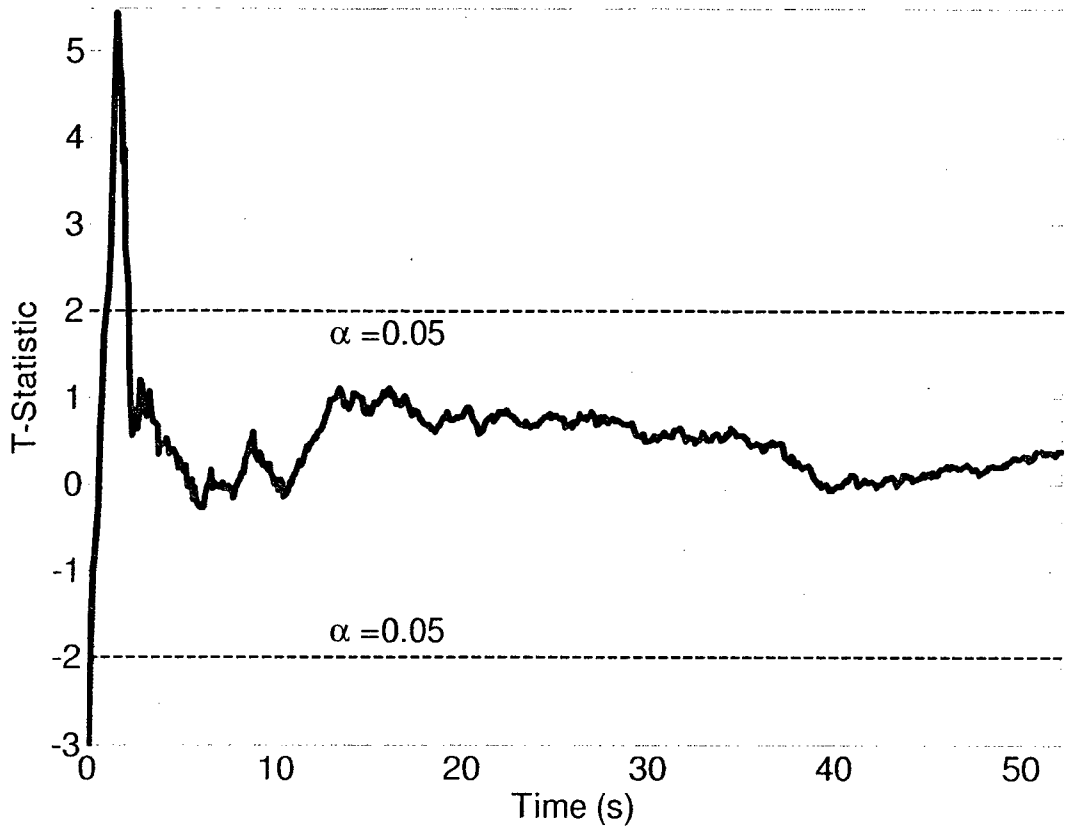


*Figure 2-6: The Two-Sample T-Statistics for the continuous time model and experimental data drilled at 30 V. The dashed lines show the critical region for a level of significance of 0.05.*

The model's variance must also follow experimental results. The model's standard deviation is fit by least squares to experimental data for standard machining at 30 V (again, as in 2.3.1.3, the 30 V experiment is taken as representative of other experiments). The computed parameters are $\mu$=10 and $\sigma$=4. Figure 2-7 shows a plot of the model's standard deviation overlaid with the experimental standard deviation, as well as the residuals from the fit.

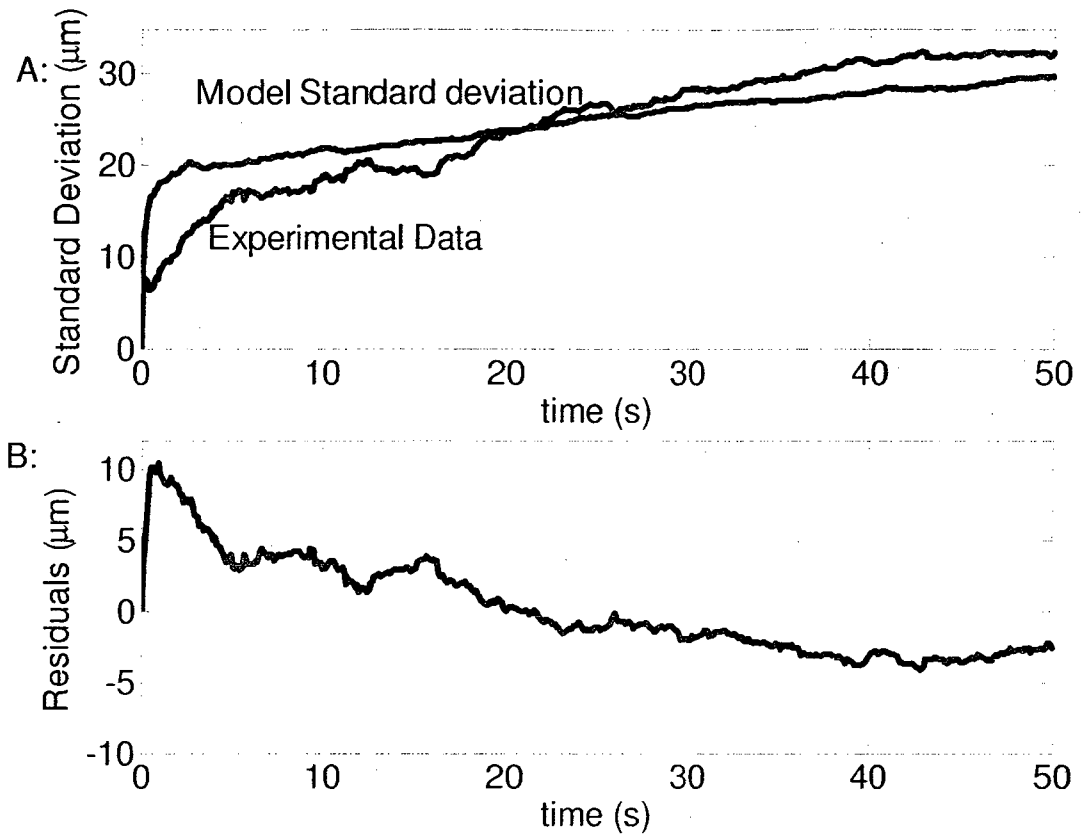


*Figure 2-7:A: Fit of standard deviation of the model to experimental data to for experiment with machining voltage of 30 V. B: The residuals.*

To quantify how close the model's standard deviation comes to the experimental data the F-statistics is used. The F-statistics for these two data sets is plotted vs. time in Figure 2-8. From the plot, it is clear that there is insufficient evidence in this case to reject the hypothesis that the two variances are the same, except for the first 10 seconds of drilling. This represents a very good match for the model. The importance of the low F-statistic in the first 10 seconds of drilling is marginalized because near the start of drilling is where the distributions involved are least likely to resemble a normal distribution, reducing the effectiveness of the F-statistics.

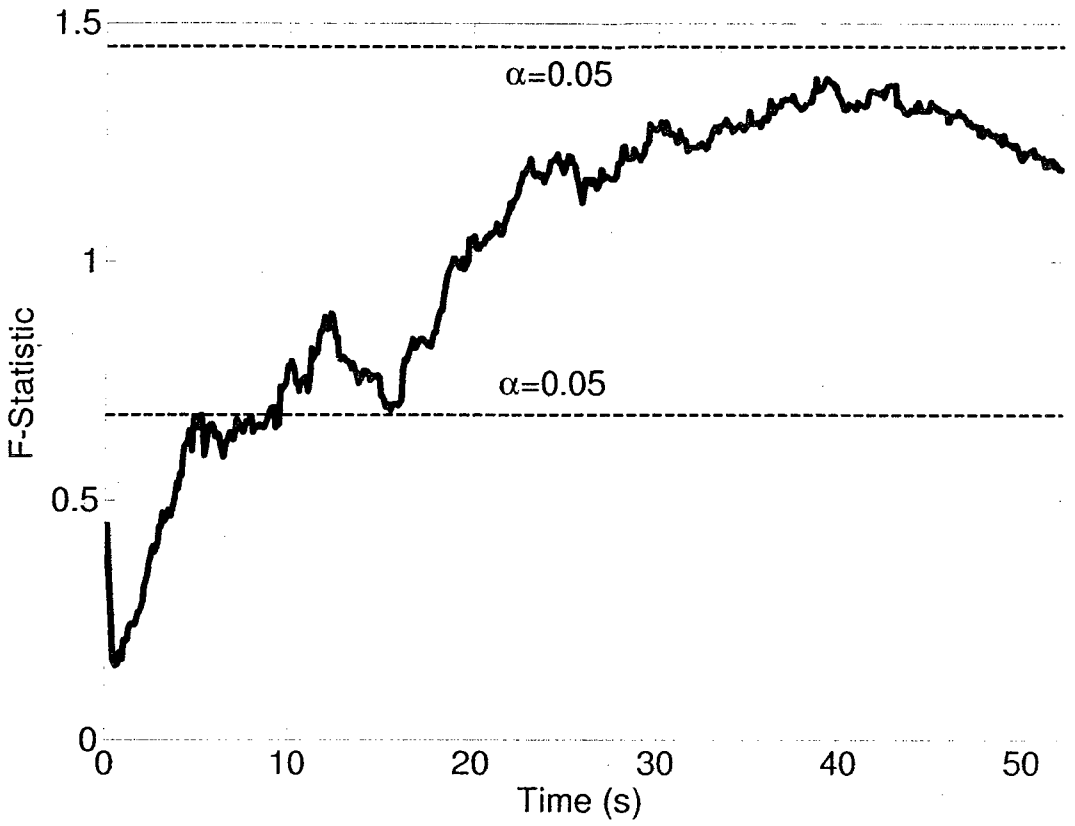


*Figure 2-8: The F-statistics for an experiment with a constant voltage of 30 V. The dashed line shows the critical region for a level of significance of 0.05.*

## 2.4 Stochastic Model (time dependent machining voltage)

### *2.4.1.1 Assumptions*

To extend both the continuous and discrete time models for constant machining voltage to time dependent voltage the assumptions from 2.3.1.1 and 2.3.2.1 are held true in addition to:

1: The mean path for changing voltage is accurately predicted by the extended mean field model of section 2.2.2.

2: Voltage only affects $v_0$ and $\mu$.

Assumption 1 allows for a less complex derivation of the time dependent voltage model. The second assumption is an expansion of assumption 2 from 2.2.2 to include $\mu$ along with $v_0$ as a voltage dependent variable. The difference between the case in this section and in 2.2.2 is the model in section 2.2.2 details a voltage dependent mean field model. Therefore there are no random jumps, and no variables $\mu$ and $\sigma$ in 2.2.2. Both could depend on voltage, but for the sake of simplicity only $\mu$ is assumed to.

The exact relationship between $v_0$, $\mu$ and machining voltage will not be studied here. The dependence will be used through a look up table and interpolation.

### 2.4.2 Discrete Time Model

#### *2.4.2.1 Formulation*

The only difference in the derivation from the constant machining voltage discrete time model is in the step where $f_d$ is solved for in (2.26) and (2.27). If the extended mean field model (2.11) is used in that step instead of (2.9) the result of (2.27) becomes

$$f_d(n, U_m) = \frac{\delta}{\mu}\left[\frac{\delta+\int_0^{n\Delta t} v_0(s)exp\left(\frac{v_{lim}}{\delta}(n\Delta t-s)\right)ds}{\delta+\int_0^{(n-1)\Delta t} v_0(s)exp\left(\frac{v_{lim}}{\delta}((n-1)\Delta t-s)\right)ds}\right] \tag{2.33}$$

instead.

### 2.4.2.2 Validation

The parameters in tables 2-5 and 2-6 are used to validate the model. The mean value is identical to the extended mean field model, so the mean value will not be tested here.

| Voltage (v) | μ (μm) |
|---|---|
| 29 | 2 |
| 30 | 2.3 |
| 31 | 3.5 |

*Table 2-5: Values for μ for the discrete time model determined by fitting the standard deviation of the model to experimental data.*

Figure 2-11 shows the F-statistic for an experiment where the voltage started at 30 V and was increased to 31 V after 30 seconds of machining. The F-Statistics is usually within the 0.05 level of significance bounds for most of the machining after the 1 V step increase. However, it remains close to the edge of the region and there is a notable period of 5 seconds where the statistics leaves the bounds. The model gives statistically significant prediction for 70% of the machining time following a voltage step.

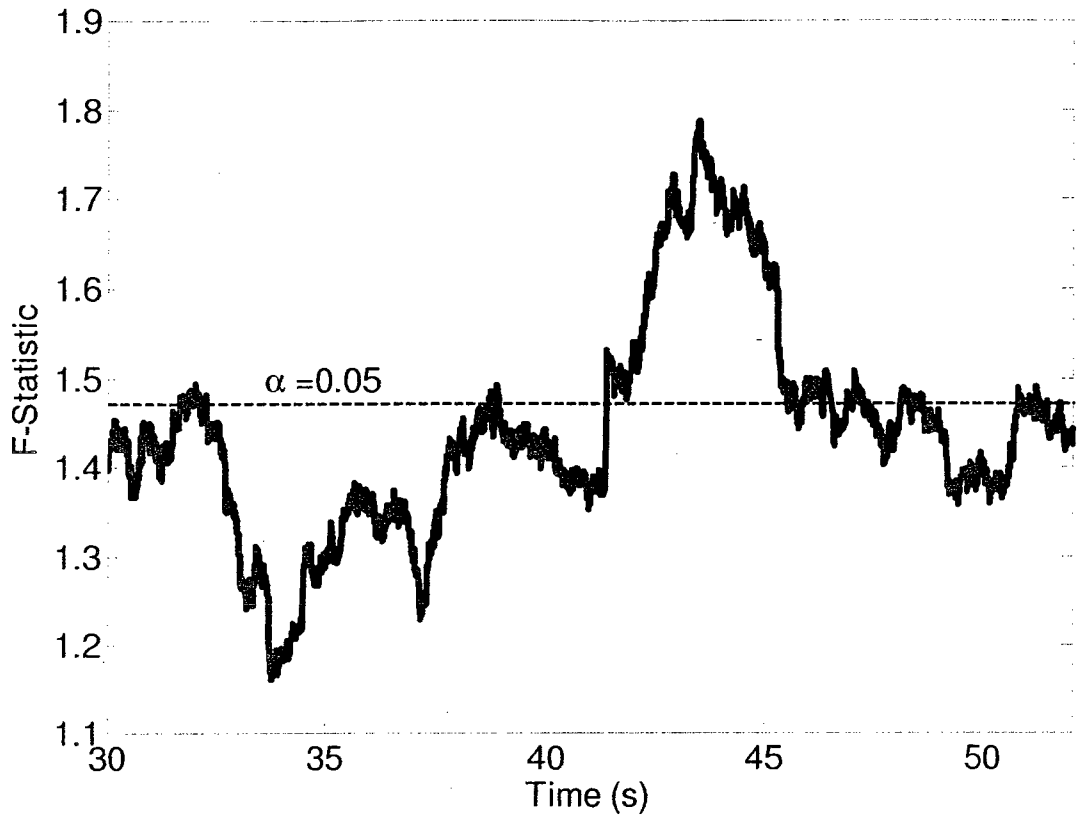


*Figure 2-9: F-Statistics for discrete time model and an experiment that used a voltage step from 30 to 31 V at 30 seconds. Dashed lines show the top of the critical range of a level of significance of 0.05.*

### 2.4.3 Continuous Time Model

#### *2.4.3.1 Formulation*

Assumption 1 means that to convert the continuous time model to work for time dependent voltages all that needs to be done is to change the equation for λ to account for the changing voltage. Thus for changing voltages (2.30) will instead become

$$\lambda(z, U_m) = \frac{(v_0(U_m) - v_{\lim})e^{-z/\delta} + v_{lim}}{\mu(U_m)}. \tag{2.34}$$

The continuous time model with time dependent voltage is depicted in the diagram in figure 2-4, where R is now a normal random variable with mean $\mu(U_m)$, instead of a constant, and standard deviation $\sigma$. Additionally, the value of $\lambda$ is now a function of machining voltage through $v_0$ and $\mu$, and is given by (2.34).

### *2.4.3.2 Validation*

The parameters in Table 2-6 are used to validate the model.

| Voltage (v) | $v_0$ (μm/s) | μ (μm) |
|---|---|---|
| 29 | 30 | 5.5 |
| 30 | 57 | 5.8 |
| 31 | 235 | 7.0 |

*Table 2-6: Values for three different voltages for $v_0$ and u determined by fitting the standard deviation of the model to experimental data.*

Figure 2-10 shows the T-statistics for an experiment whose machining voltage was 30 V at the start, and switches to 31 V after 30 seconds of drilling. A value of T-statistics closer to one indicates it is more likely that the two distributions posses the same mean value. The two dotted lines on the figure represent the critical values for a level of significance of 0.05. After the jump at 30 seconds, it is not possible to reject the hypothesis that the mean of the model and the experiment agree with a level of significance of 0.05, indicating a good match between experiment and model.

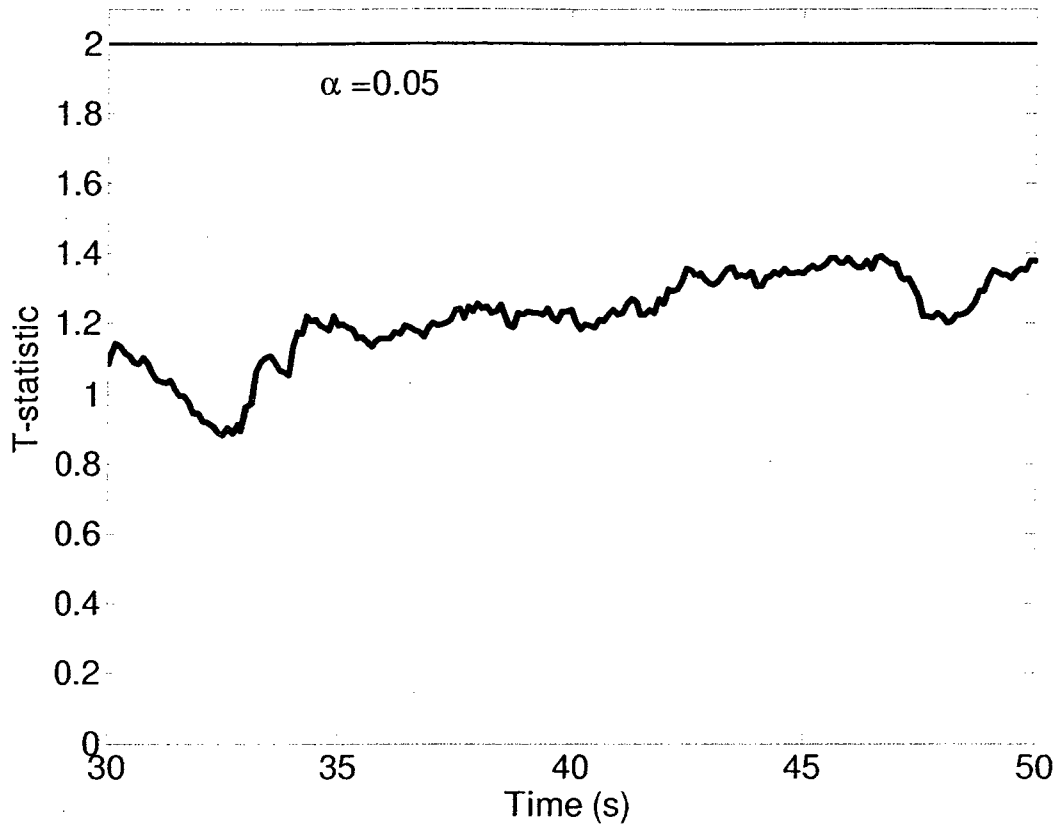


*Figure 2-10: T-statistics for a voltage step from 30 to 31 V. Dashed lines show the critical values of a level of significance of 0.05.*

Figure 2-11 shows the F-statistics for the same experiment used for figure 2-10. It is clear that the F-Statistics is well within the 0.05 level of significance bounds. Being within the bounds means that it is not possible to reject the hypothesis that the variances are the same with a level of significance of 0.05.

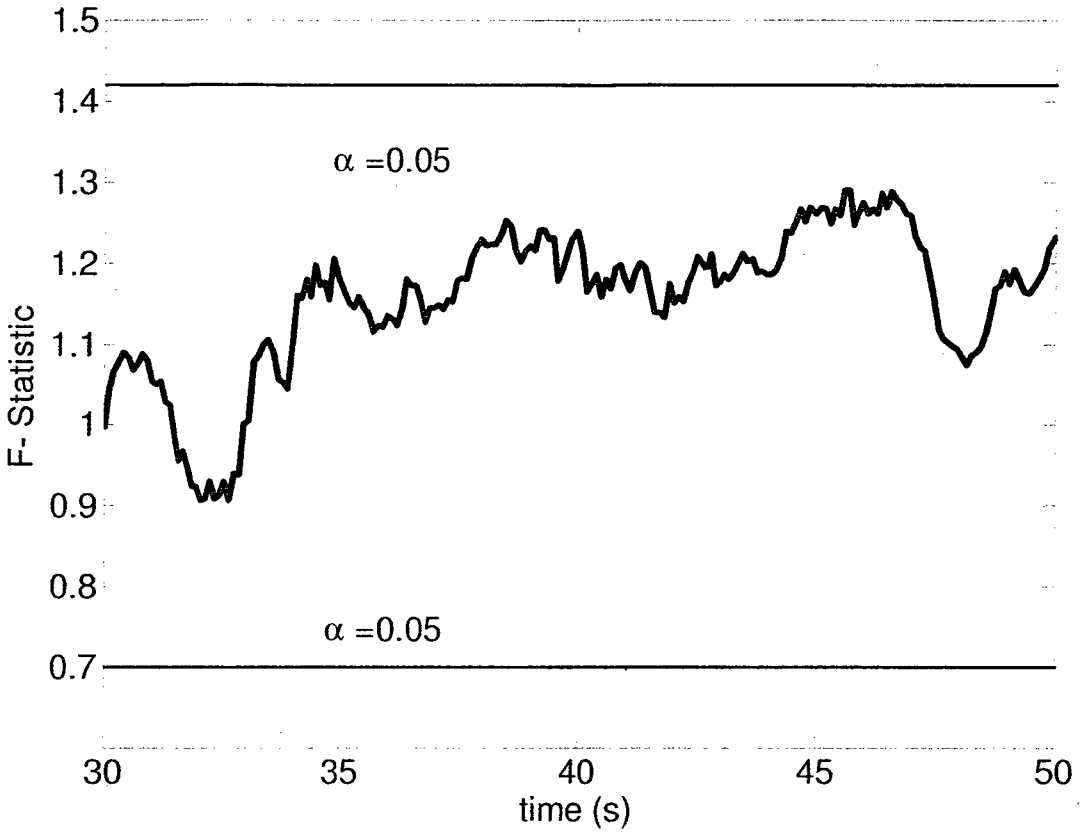


*Figure 2-11: F-Statistic for a voltage jump from 30 to 31 V. Dashed lines show the critical values for a level of significance of 0.05.*

## 2.5 Conclusions

The models derived here were validated by comparison with the state of the art mean field model, as well as with experimental data. For both discrete time and continuous time models, and for both constant voltage and time dependent voltage, there was no significant difference between the modeled mean and standard deviation and experimental results for the cases considered, except for the initial transient time after changing the voltage, for a level of significance of 0.05.

The models are also seen to accurately predict the general shape of the coefficient of variation plots generated from experimental data. Experimentally, the coefficient reaches a steady state value after an initial decrease. Both models reproduce this behaviour. The steady state value of the coefficient of variation could be used as a single number to efficiently compare the variability between two experiments. Alternatively, the model parameters, the jump-mean and the jump-standard-deviation can be used to compare variability between two experiments that posses similar mean value curves.

# 3 Variability in SACE Gravity Feed Drilling

The variability of SACE gravity feed drilling is investigated in this chapter through experimental results. First discussed is the SACE machining set-up used for all the experiments presented in this thesis. The standard experimental method is explained, and modifications to the standard procedure are outlined, such as using electrolyte level control.

The variability is examined in terms of the coefficient of variation (2.3). As explained in chapter 2, the coefficient of variation is useful for examining variation of two distributions which have significantly different means, a quality that is very useful here. The experimental results shown support the prediction from chapter 2 that the coefficient of variation reaches a steady value.

The effects of regulating the temperature and electrolyte level in a more detailed manner than in the standard experiment are investigated. It is found that preheating the electrolyte to its known steady state temperature cuts the coefficient of variation in two. A similar result is obtained if the electrolyte level can be maintained to within ±0.05mm. When both procedures are combined the steady state value of coefficient of variation is decreased even further, to 30% of the standard experimental value. Additionally, vertical vibration of the tool electrode during machining is seen to have no effect on the variability, which is useful because vibration also increases the speed.

## 3.1 Introduction

### 3.1.1 Variability due to Bulk Temperature of Electrolyte

The bulk temperature of the electrolyte is known to have an effect on the SACE drilling process [13]. However, in general no care is taken to regulate the temperature of SACE drilling, which is interesting because most of the energy used in the process goes into heating the electrolyte (as opposed to machining) [31], thus raising its temperature as consecutive holes are drilled. Some studies have compensated for non-controlled temperature in the electrolyte in their analysis by discarding the first ten holes [3, 16]. However, the effects from those studies are attributed to changes in *local* temperature (close to the tool) as opposed to non-constant *bulk* temperature (far from the tool).

### 3.1.2 Variability due to Level of Electrolyte

The level of the electrolyte above the work piece is known to affect the SACE drilling process [3]. However, this effect is only known in the sense that a low level of electrolyte is different from a high level of electrolyte. During machining, the level of the electrolyte in the processing cell drops. This occurs due to evaporation and splashing, which are both caused by the SACE drilling process. However, no effort is made to regulate the electrolyte level. Generally the process cell is filled for a set of experiments, and not considered after that. Further, either the electrolyte level is not mentioned in reports (e.g. [11]), or it is mentioned only as an approximate starting value (e.g. [21]).

### 3.1.3 Coefficient of Variation

The coefficient of variation is used to compare the variability between two different sets of holes. The coefficient of variation is defined by (2.3). It is useful for comparing

variability between two distributions when their mean values differ significantly. This is often the case when comparing sets of holes drilled with SACE gravity feed drilling. Various modifications to the SACE process can have an effect on the mean value as well as the variability.

## 3.2 Experimental Set-up and Procedure

### 3.2.1 Experimental Set-up

The SACE set-up used for this work can be broken down into a few major components. One component is the motion platforms, 3 precision motion axes are used to position the work piece with respect to the tool electrode. There is also the processing cell, where the machining occurs, and the tool head, the structure which the tool electrode is attached to. The entire set-up is seen in Figure 3-1.

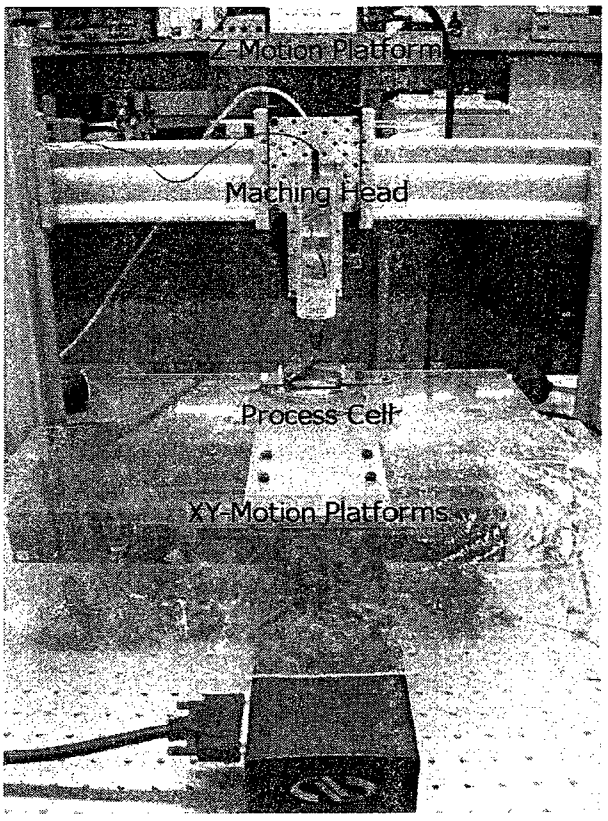


*Figure 3-1: The SACE machining set-up. The process cell, where machining takes place, is mounted on a set of xy-motion platforms. The machining head, which is what the tool electrode is attached to, is fixed to a vertical motion platform.*

The processing cell, holding the work piece, consists of a circular reservoir for the electrolyte. The inner wall is covered by a stainless steel ring, which acts as the counter electrode for the SACE process. Built into the reservoir are two clamps that hold samples in place for machining. The processing stage is mounted onto a two axis precision motion stage, which allows for positioning in the horizontal plane. The processing cell is seen in Figure 3-2.

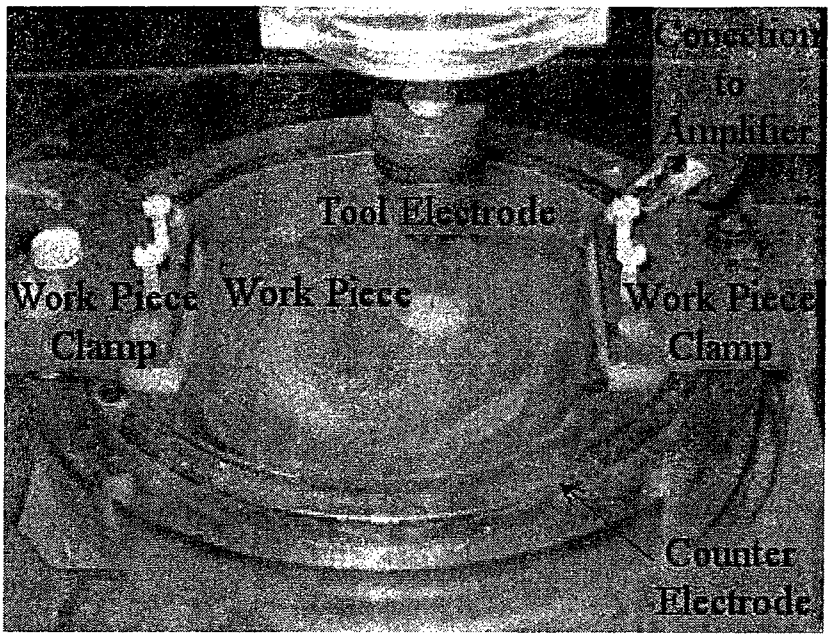


*Figure 3-2: The process cell during machining. The work piece is held between two clamps which secure it for machining. The counter electrode is a piece of steel encircling the side wall of the cell, as it attached to a wire that goes to the power amplifier.*

The machine head's main purpose is to hold the tool electrode. The tool electrode, a 0.4mm stainless steel rod, is attached via a drill chuck which screws onto a structure that is free to move vertically over a range of 1.5mm. The flexible structure is mounted on the vertical motion platform. There are two other important features of the machine head. First, the machine head has an optical sensor that measures the flexible structure's current vertical position relative to the rest of the machine head. Second, a voice coil actuator can apply a force to the flexible structure. The entire structure is fixed to vertical motion platform. The machine head is seen in Figure 3-3.

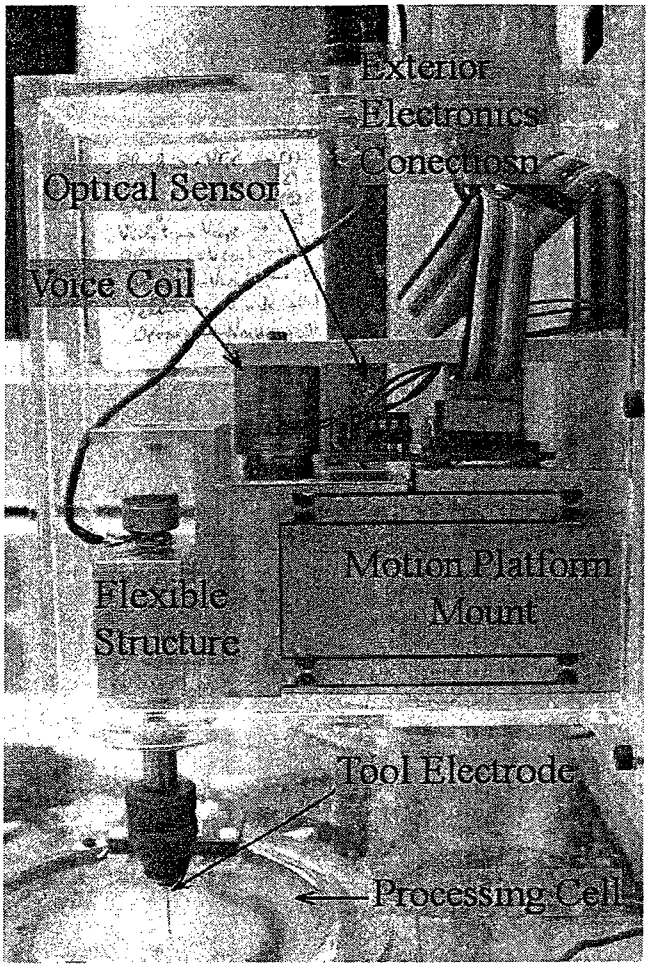


*Figure 3-3: The machine head during machining. The entire structure is mounted to the z-motion platform. The tool electrode is attached to a flexible structure that is free to move vertically. The voice coil and optical sensor are above the flexible structure. The coil can be used to apply a force to the flexible structure, while the optical sensor measures the flexible structures position.*

A Newport XPS motion controller moves the three precision stages and gathers data from the optical sensor incorporated in the machining head. The XPS is also connected to a power amplifier (Avtech AV112-D) that supplies the desired machining voltage to the processing cell. Machining is done in the cathodic mode (tool-electrode is polarised as a cathode). There is a negligible resistance between the output at the amplifier's terminals

and the tool- and counter-electrodes. The amplifier has a bandwidth of 20 kHz and is capable of a peak power output of 250 W.

### 3.2.2 Experimental Procedures

#### *3.2.2.1 Standard experimental procedure*

The experiments done were all SACE gravity feed drilling, with a constant force of 0.8N applied on the tool-electrode, or modification thereof. The work-pieces are microscope glass slides (VWR VistaVision slides) and the electrolyte is 30% wt NaOH prepared from deionised water. The same volume of electrolyte is used in each experiment to ensure the electrolyte level above the work-piece is consistently at 2mm at the start of each experiment. After positioning the tool-electrode above the desired micro-hole location, the vertical platform lowers the machine head. The machine head is lowered until the flexible structure (where the tool is mounted) has risen 1mm, relative to the machine head. A constant voltage is applied between the tool- and counter-electrode for 55 seconds. During this time, data from the optical sensor is recorded. Since during gravity-feed drilling the tool is always in contact with the bottom of the hole, this data shows the hole's depth evolution. Note that in cathodic SACE machining, the tool wear is very small and does not present a significant source of error [2, 5]. A complete experimental set consists of drilling 52 holes. Also note that in general the electrolyte will have lowered by 0.9±0.2mm over the course of the experiment due to lose of electrolyte from splashing and evaporation.

### *3.2.2.2 Modified experimental procedures*

The basic apparatus and procedure described above were modified in several ways for this work. The modifications are:

1. **Machining with electrolyte level control.** In electrolyte level control, a stainless steel piece which is termed in the following as the overflow electrode, is tightly clamped on top of the work piece.

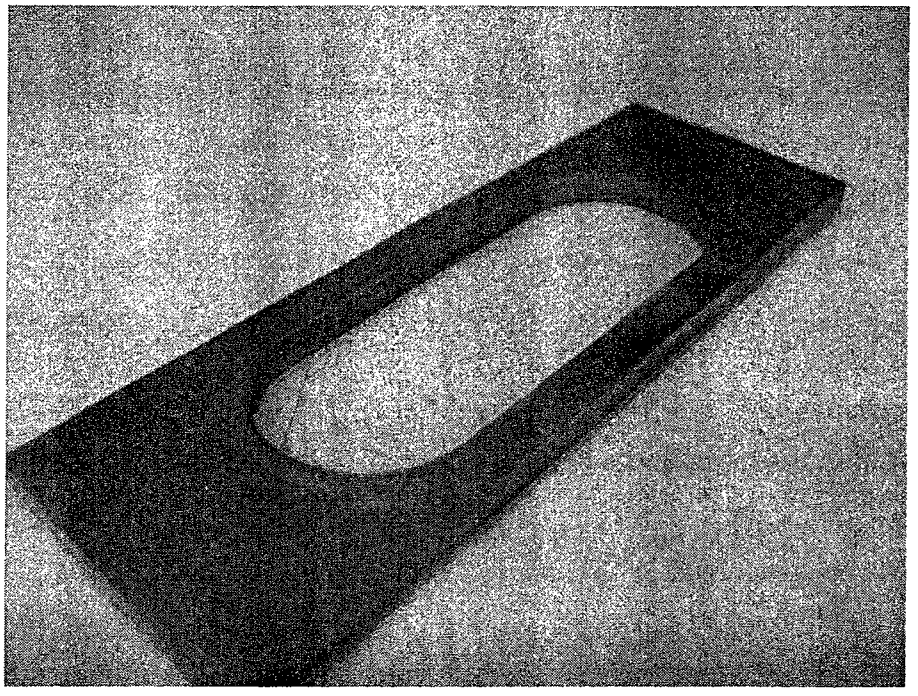

*Figure 3-4: The overflow electrode.*

This overflow electrode is used as the counter electrode instead of the metallic wall of the processing cell. Electrolyte is added until the electrolyte overflows the edge of the overflow electrode. This ensures that the electrolyte level is at the same height after each refill. The contact between the overflow electrode and the work piece is tight enough that no electrolyte escapes this tiny reservoir.

Additionally, the electrolyte in the hole is flushed out and refilled every third hole. In combination with the overflow effect, this ensures that, while using level control, the level of the electrolyte remains at 2mm ±0.2mm. The error corresponds to the average decrease in electrolyte level over the course of 3 holes. Electrolyte is lost faster than the standard experiment because of the smaller volume.

2. **Machining with preheated electrolyte.** In the preheated electrolyte variant, any electrolyte added to the experiments has been preheated to 61° C. This temperature was chosen because it is the steady-state value of the electrolyte bulk reached during standard SACE machining in the set-up used by the author.
3. **Machining with tool-electrode vibration.** Tool-vibration is achieved by driving the input of the voice coil on the machine head with a function generator. The desired amplitude and frequency of vibration is selected by tuning the function generator while observing the optical sensor data on an oscilloscope.

## 3.3 Effect of Preheated Electrolyte

Preheating the electrolyte to 61°C before starting a SACE experiment (as explained in section 3.2.2.2) substantially reduces the coefficient of variation as shown in figure 3-5.This suggests that a large portion of the cause of variation in regular SACE drilling is due to insufficient control of the bulk temperature of the electrolyte. Note also that the coefficient of variation reaches a steady-state value similar to the standard case and does so in a similar amount of time.

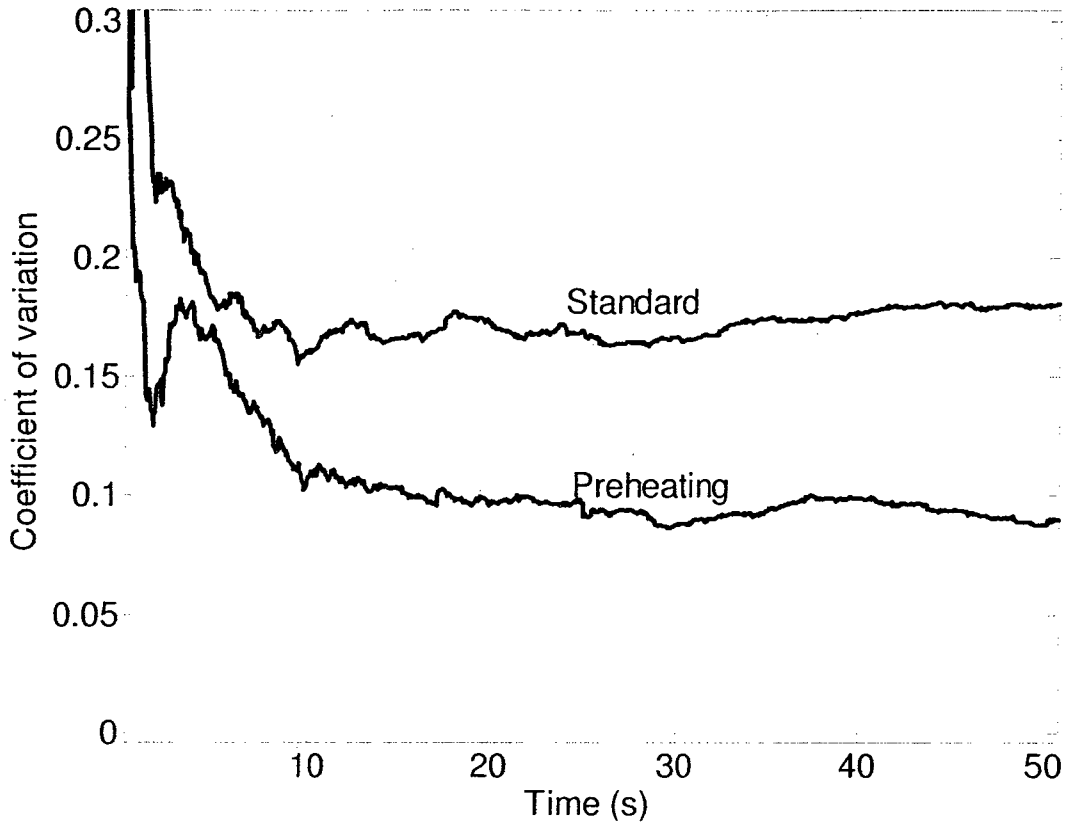


*Figure 3-5: Coefficient of variation for both an experiment with preheated electrolyte and an experiment using the standard set-up.*

Figure 3-6 offers an explanation of why preheating of the electrolyte to 61° C leads to a reduction in the coefficient of variation. Figure 3-6 a, and b are run charts of the depth drilled by the process after 25 seconds. It can be seen in those two plots that in the standard process there is a transient from hole to hole, where later holes are drilled faster. Also note that the two run charts for the standard process have different patterns. The run chart in figure 3-6 a has a short and fast transient which then levels off to a steady state (consistent with what was reported in [16]), while Figure 3-6 b shows a steady increase in speed of drilling. Although the exact nature of the transient seen in the standard

experiment changes, the speed always increases from the start to the finish. Also note, the variability is similar between sets of holes. Figure 3-6 c is a run chart for an experiment where preheated electrolyte is used. It shows no signs of a transient similar to the ones for the standard experiment; this is a repeatable result. The lack of the transient in the preheated electrolyte experiments is the reason they have lower standard deviation.

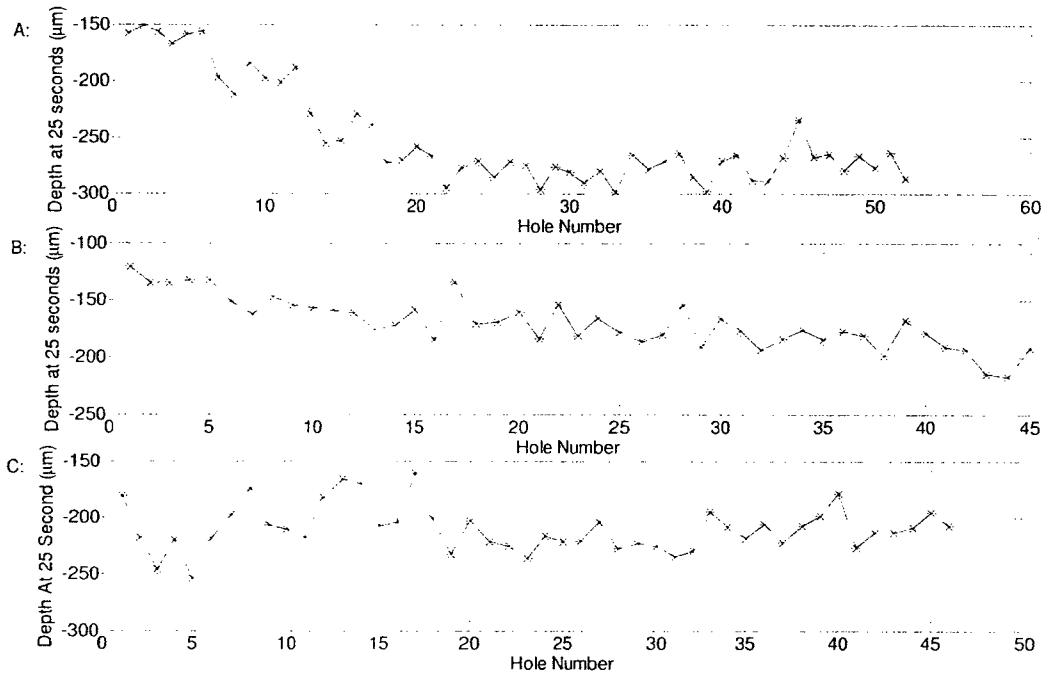


*Figure 3-6: Run chart of depth drilled after 25 seconds for A,B: a standard experiment, C: an experiment using preheated electrolyte. Note the decreasing trend in A and B, which is absent in C.*

Another interesting element to note about the effects seen from preheating the electrolyte is that the bulk electrolyte temperature in the preheated case is only approximately 40° hotter than the standard case. The difference in speed seen between early holes and later

holes is consistent with the model for initial speed shown in [1]. The initial velocity of drilling depends on temperature through $\kappa$, the normalized heat power

$$\kappa = \lambda_d \cdot \frac{h_d q_E}{\lambda_c (T_M - T_0)}, \tag{3.1}$$

where $\lambda_d$ is the mean rate of discharges, $\lambda_c$ is the thermal conductivity of the work piece, $h_d$ is the height of the tool over which discharges (which directly relate to the electrolyte level) occur, $q_E$ is the amount of heat transferred to the work piece per discharge, $T_m$ is the temperature at which machining occurs and $T_0$ is the bulk temperature of the electrolyte (i.e. the temperature far from the tool). If $T_m$ is assumed to be 600°C [11], rising $T_0$ from 20°C to 60°C causes an increase in $\kappa$ by a about ten percent. Based on experimental results from [11], such an increase could cause an increase in initial velocity typically between 20 μm/s and 60 μm/s. A higher original initial velocity will cause larger increases. Higher original initial velocities could result from high voltages, low electrolyte depth, etcetera. The order of magnitude of the change in speed predicted by the model from [11] is consistent with what is seen in the run charts. Since the model is based on the idea that machining is through chemical etching occurring at 600°C, this serves to bolster the evidence that chemical etching is the main mechanism of machining in SACE.

## 3.4 Effect of Electrolyte Level

### 3.4.1 Without Electrolyte Preheating

Electrolyte level control (as explained in 1) increases the value of the coefficient of variation (Figure 3-7). In addition to this, a much slower decrease from the initial value is observed. Also seen in the figure is the coefficient of variation taken from the data of only every third hole (i.e. only data for holes directly after electrolyte is added. It is called the every-third-hole subset of data). In the every-third-hole subset of the level control data, the steady state coefficient of variation is lower than the standard case. The electrolyte levels at every third hole will be almost identical to each other. Thus, the every-third-hole coefficient of variation shows how much the variation can be decreased if the electrolyte is limited to be within ±0.05mm. The overflow electrode keeps the level with ± 0.2 mm overall (see 3.2.2.2), but the level directly following an electrolyte refresh is more consistent than that, which is where the ±0.05mm number comes from.

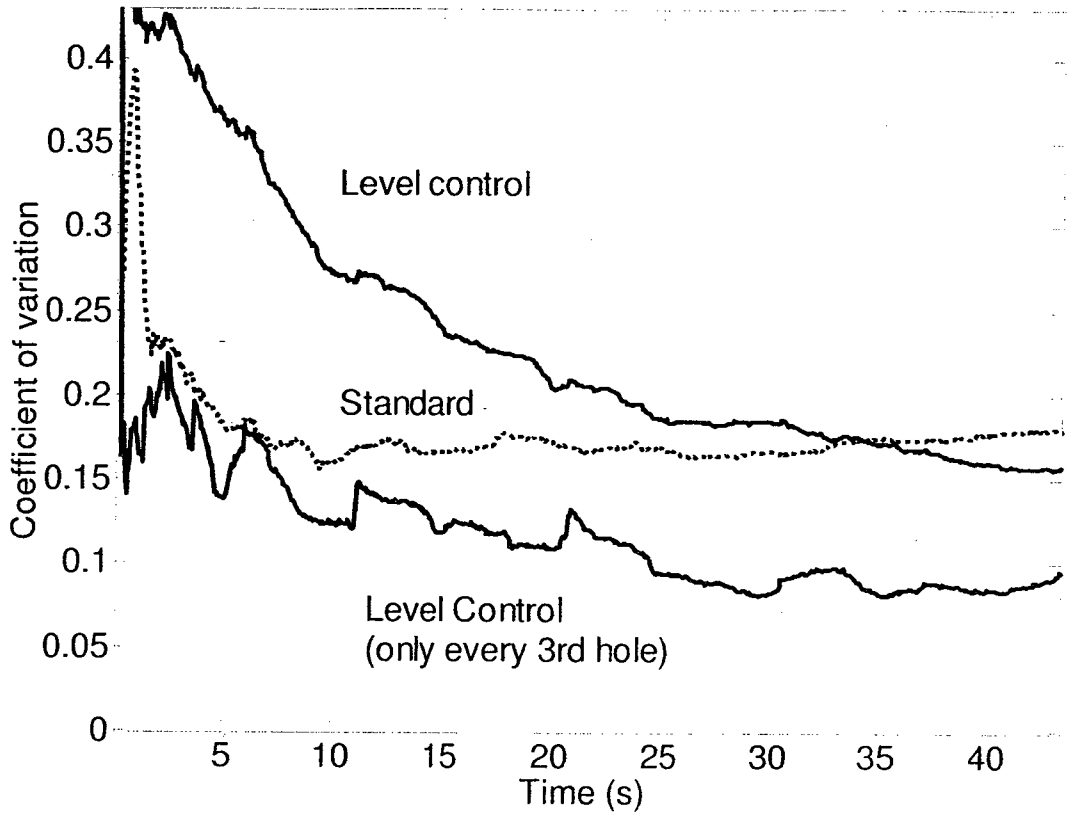


*Figure 3-7: Coefficient of variation for an experiment using electrolyte level control. Also displayed the coefficient of variation for a standard experiment (dotted), and a the coefficient of variation for every third hole of the level control experiment. Every third hole corresponds to all the holes directly after new electrolyte is added.*

The reason why looking at only every third hole makes a large difference is seen in figure 3-8, a run chart for the level control experiment. There is a clear oscillating pattern whereby the holes that are drilled directly following the addition of electrolyte (circled on the graph) are drilled slower than the following two holes. There are a couple possible causes of the increase in speed from the first hole after a refreshing of the electrolyte, to the following two. First, the bulk temperature of the electrolyte will increase as heat is added to it from the process. The higher bulk temperature will lead to faster drilling. Also, electrolyte is lost from the container during drilling, and a lower electrolyte level is known to increase drilling speed. The oscillatory behaviour can be attributed to a

combination of the increase in temperature and the decrease in electrolyte level. However, without further information the effect of these two sources cannot be separated.

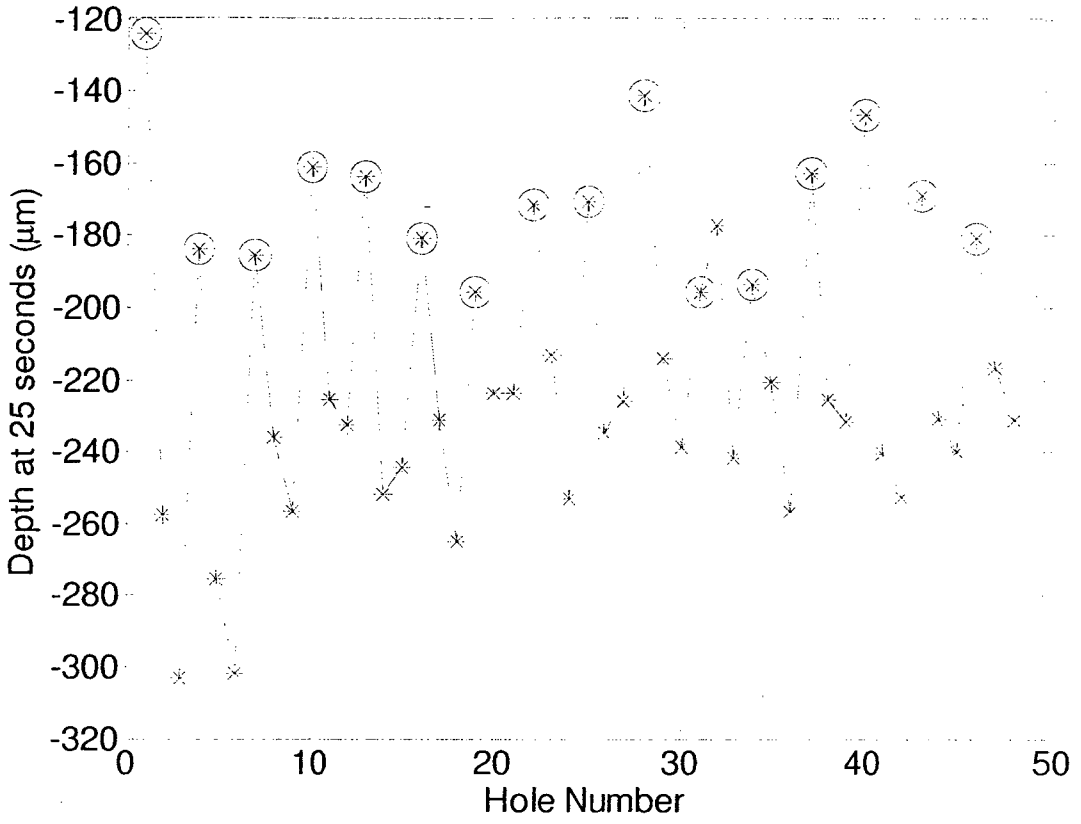


*Figure 3-8: Run chart for electrolyte level control experiment. Circled points correspond to holes drilled directly after electrolyte was refreshed. Note the oscillating pattern which matches with when electrolyte is added; drilling speed is slowed down after addition of electrolyte then increases.*

### 3.4.2 With Electrolyte Preheating

When electrolyte level control is combined with electrolyte preheating the coefficient of variation achieved considering all holes in the experiment is the same as using just preheating. This shows that having a variability in the electrolyte level of ±0.2mm with preheating is not significant. However, if the set of data is reduced to only every third hole (as in the previous section, only the hole directly following addition of electrolyte

are considered), there is a significant decrease in the coefficient of variation. The steady state coefficient of variation is approximately 30% of the standard case; this is better than either just preheating or just level control.

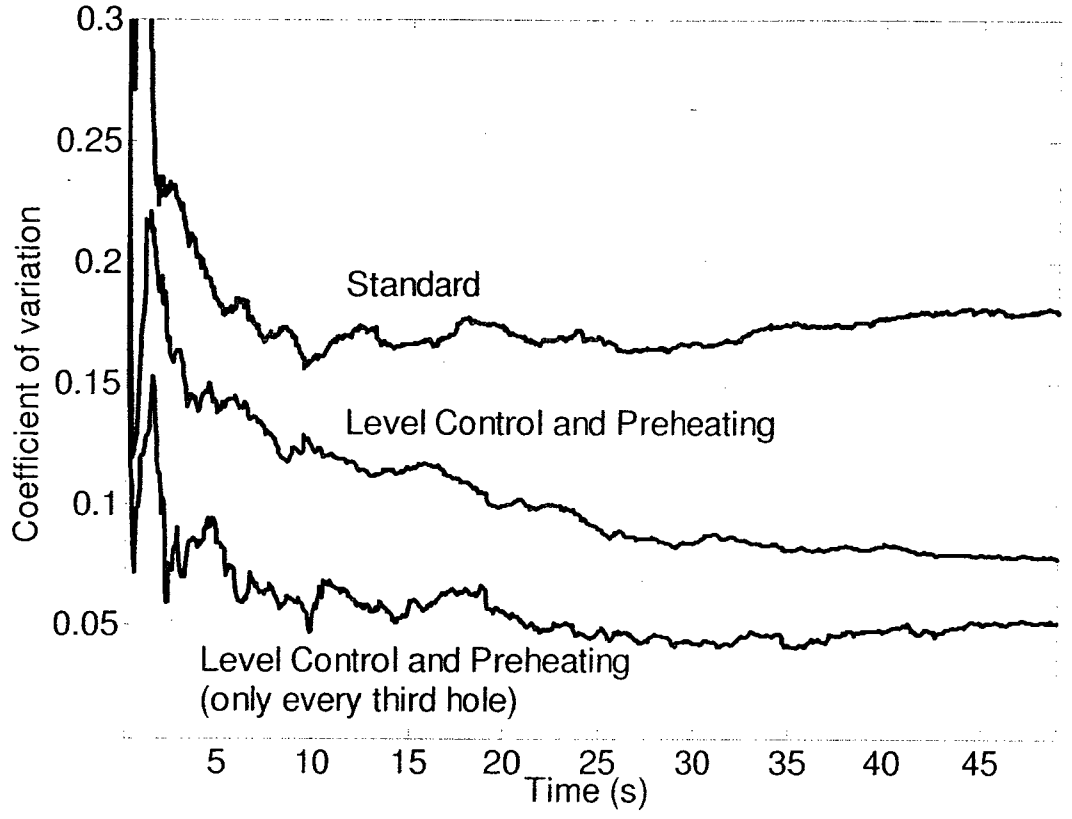


*Figure 3-9: Coefficient of variation for an experiment using electrolyte level control with preheating. Also shown is the coefficient of variation for the standard experiment, and a the coefficient of variation for every third hole of the level control experiment. Every third hole corrisponds to all the holes directly after new electrolyte is added.*

Figure 3-10 shows a run chart from the data used for figure 3-9. There is still the oscillating pattern seen with the level control (without preheating) experiment. An interesting difference between figure 3-10 and figure 3-9 is that in the case where both electrolyte level control and preheating are used, the difference between the first hole

after refilling and the second is almost the same as between the second and the third. However, when just level control is used, the difference between the first and second holes is much greater than between the second and third. The explanation of this is that: the electrolyte level changes over the three holes consistently, whereas the temperature increases more between the first and second holes than between the second and the third holes. Thus, adding preheating to the level control experiment has successfully removed most the variation due to temperature.

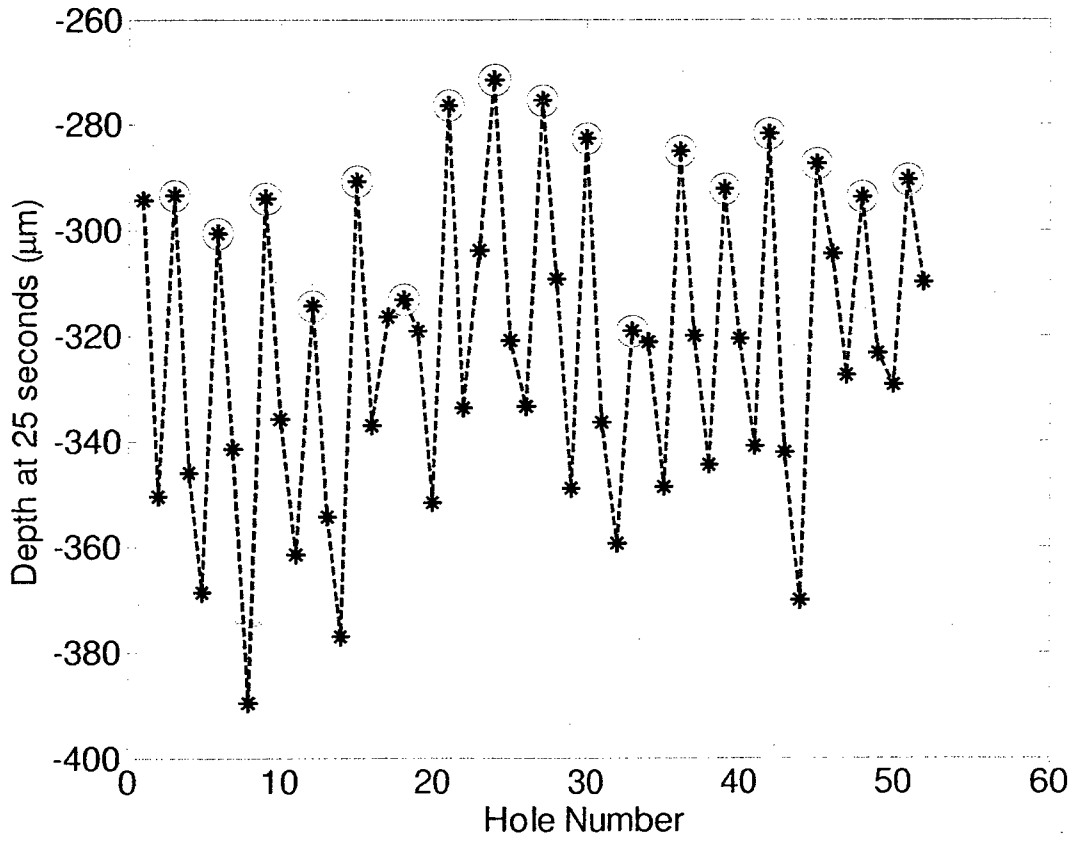


*Figure 3-10: Run chart for experiment done with electrolyte level control and preheated electrolyte. Circled points corespond to holes drilled directly after preheated electrolyte is added. Note the oscillating pattern which matches with when electrolyte is added; drilling speed is slowed down after addition of electrolyte then increases.*

## 3.5 Effect of Vertical Tool Vibration

In both, the standard case and the case of electrolyte level control and preheating, no clear increase or decrease is seen when tool vibration is employed (Figure 3-11 ). From a practical point of view, this is an interesting result: tool vibration does not increase the process variability while at the same time it increases the average drilling speed [19].

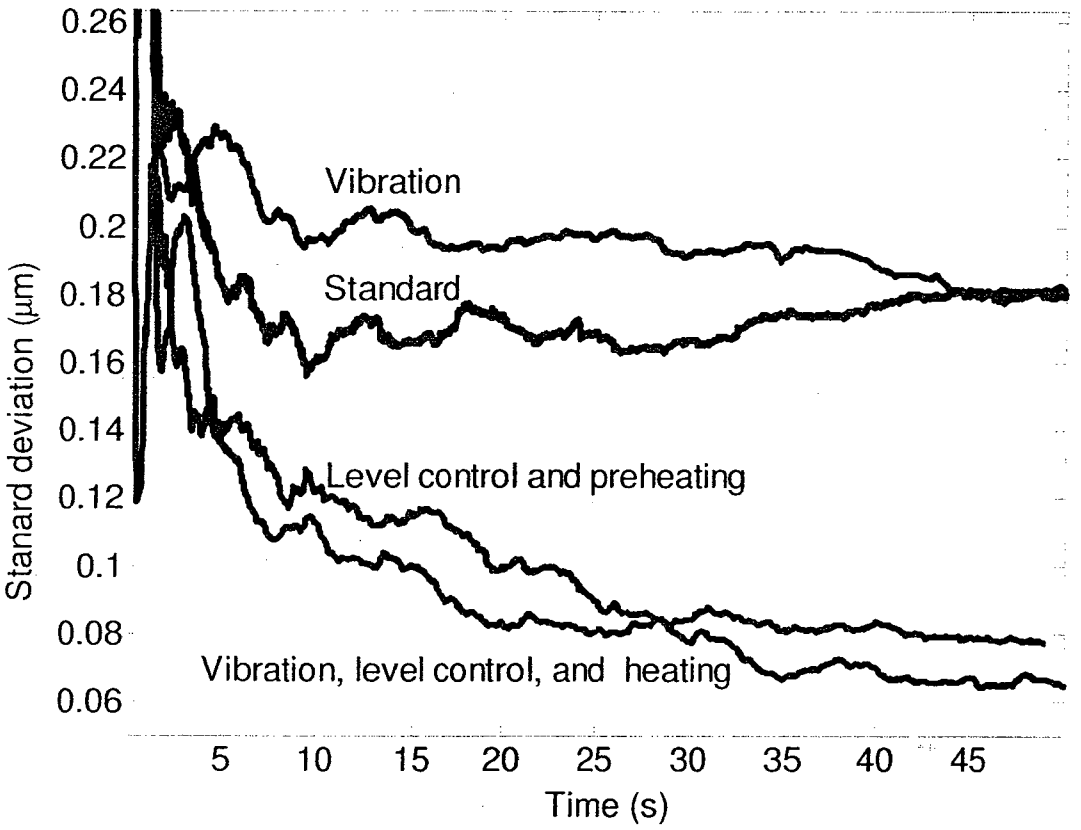


*Figure 3-11: Coefficient of variation for drilling with 10 μm at 30 Hz tool vibration (depth evolution data for vibration experiments was low pass filtered at 10hz). Shown in the plot is the coefficient of variation for a standard experiment, an experiment with both electrolyte level control and preheating, a standard experiment with tool vibration, and an experiment with electrolyte level control, preheating, and tool vibration.*

## 3.6 Summary

The effect of the variability in the electrolyte's bulk temperature is quantified. Preheating the electrolyte to the steady state temperature it reaches during normal machining (61°C) results in a decrease in the stead state value of coefficient of variation by half. Additionally, the amount of variability due to uncontrolled temperature agrees with a previously developed model for drilling speed based upon the assumption that chemical etching is the primary machining mechanism.

The effect of variable electrolyte level on the variability of the process is also quantified. It is possible to reduce the coefficient of variation to half the value seen in the standard case, if the electrolyte level is maintained at almost exactly the same level (±0.05mm). Additionally, when preheating electrolyte is combined with electrolyte level control, the effect is to reduce the coefficient of variation to 30% of the value seen in the standard experiment.

Finally, the effect on the coefficient of variation of using tool vibration is examined. No significant difference is seen between the tool vibration case and the standard case. This is important because tool vibration accounts for an increase in speed, without a corresponding increase in variability.

The findings of this chapter are summarized below in Table 3-1.

| Experiment | $c_v$ steady state value for standard process | $c_v$ steady state value for process with level control and preheating |
|---|---|---|
| Standard | 0.18±0.02 | 0.05±0.005 |
| Level Control | 0.1±0.02 | N/A |
| Preheating | 0.09±0.01 | N/A |
| Vibration | 0.19±0.01 | 0.07±0.005 |

*Table 3-1: The values of the steady state of coefficient of variation. Error bounds are estimate based on how much noise is seen in the coefficient of variation once it has reached a steady state.*

# 4 Reduction of Variability

Feedback control applied to the SACE gravity feed drilling is examined in this chapter. Several signals that can be used as sensor signals or actuator signals are discussed. Then, the results of applying two different feedback controllers are presented. These results are compared to the prediction of the model presented in chapter 2.

The first controller to be examined is a proportional feedback controller. It is able to reduce the variability of the machining process by a factor of three in standard SACE gravity feed drilling, and by a factor of two when electrolyte level control and preheating are employed. However, the final result in both cases shows a similar steady state coefficient of variation. The model's prediction matches the results for the lower gain, but for higher gains the agreement is not very accurate.

The second controller is based on the voltage-depth quality relationship Figure 1-5 from [16]. The voltage is set as a function of depth, decreasing with depth, and always staying in the "smooth surface" depth-voltage zone. It is also able to reduce the coefficient of variation, although the justification cannot be made based on the model of chapter 2.

## 4.1 Introduction

The final goal of any control scheme for SACE drilling must be to increase the quality of the micro holes, which is the finished product. However, the quality of the micro-holes can only be judged off-line, after drilling. Unfortunately, when the process is finished, it is too late to take any action to correct the hole. Correlations between parameters that can be measured online and the final quality of the hole must be discerned to create a better control scheme for SACE drilling. In addition to this, a manner in which the on-line

measurable quantities can be regulated must be known. The former of the two problems is the focus of this chapter.

## 4.2 Feedback control in the context of SACE

In this section a non-exhaustive list of potential signals that could be used in a control system for SACE drilling will be examined. Signals that can be used to measure the system will be examined (referred to as "sensor signals" hereafter) first, followed by an examination of signals that could be used to actuate the system (referred to as "actuator signals" hereafter). The signals will be further classified according to which of the following categories they fall under:

- Electrical: Signals related to the properties of the electrical circuit.
- Mechanical: Signals related to physical motion of the tool.
- Electrolyte: Signals related to the physical and chemical properties of the electrolyte.

Table 4-1 lists potential feedback and actuator signals.

| | Electrical | Mechanical | Electrolyte |
|---|---|---|---|
| **Sensor:** | Current | Depth | Local Temperature |
| | | Force | |
| | | | |
| **Actuator:** | Voltage: | Force | Bulk Electrolyte Properties |
| | Arbitrary Waveform | Feed Rate | |
| | Square Wave Properties | Tool Rotation Properties | |
| | | Tool Vibration | |

| | Properties | |
|---|---|---|

*Table 4-1: Classification of feedback and actuator signals.*

### 4.2.1 Sensor Signals

**Current:** The current drawn by the system has been examined specifically for its use as a sensor signal [17]. Discharge events are identifiable in the high frequency range of the current signal. However, there is no clear link between the discharge events and the machining status [17]. It is thought that, potentially, further information could be combined with the current signal to elucidate more information about the machining status. The low bandwidth information from the current signal allows the determination whether a gas film is present around the tool or not, and so, whether machining is occurring [17, 32].

**Depth:** This signal can only be used as a sensor signal in gravity feed drilling. This is because it relies on the special property of gravity feed drilling that the tool remains in contact with the bottom of the hole throughout drilling.

**Force:** This signal can be used as a sensor signal only in the case of constant velocity drilling; in gravity feed drilling the force is set as a parameter. So far two methods where used to measure the force during drilling: a force sensor, based on the zero displacement method, directly incorporated in the machining head [33] and a loadcell placed under the work piece [25]. Systematic characterisation of the force during constant velocity feed drilling was done recently [34]. The force has been used to prevent tool bending in constant velocity drilling by briefly stopping the motion of the tool if the force measured

is above a threshold [33]. It has been suggested that this practice can also produce higher quality holes [25], but no direct comparison with other methods has been made.

**Local Temperature:** The local temperature is known to increase directly following a discharge event [31]. This suggests that comparable information can be determined from it as can be deduced from the current signal. The set-up used in [31] is only capable of measuring the temperature when it exceeds 815°C. This makes it possible that a set-up capable of reading lower temperatures could determine more information.

### 4.2.2 Control Signals

#### *4.2.2.1 Electrical*

**Voltage (Arbitrary Waveform):** The machining voltage can be set to arbitrary values (possibly limited to be within a range) at each instant in time. Using the voltage as an actuator signal would be straightforward to implement in most SACE drilling set-up. All that would be needed to be done is to exchange the DC voltage supply with a power amplifier. Changing the voltage could be very fast compared to the speed of drilling, but this would depend on the amplifier used.

So far, using time dependent voltage has not been studied for SACE drilling (except specific wave forms discussed below). However, the effect of constant voltage at different levels is known. Higher machining voltage produces faster drilling [13]. The effect of voltage on speed decreases exponentially as depth drilled increases [11]. If constant voltage is used the quality of a hole can be predicted based on the depth drilled, and the voltage employed [16].

**Voltage (Square Wave):** Instead of allowing the voltage to take arbitrary values at each instance in time, the voltage can be constrained to be a square wave. The square wave would have certain amplitude, offset (from zero), frequency, on time, off time, duty cycle, etc. Using one or more of these parameters as an actuator signal is possible (although some are mutually exclusive). Voltage pulses can affect the speed of drilling, as well as the vertical cross section of the holes, and the smoothness of the walls [21-23].

#### *4.2.2.2 Mechanical Signals*

**Force:** If a gravity-feed drilling method is used, the force applied to the tool can be used as an actuator signal. Modulating the machining force could be done quickly compared to the speed of the process, though not as fast as modulating the voltage. A higher force will increase the speed of drilling, and has an effect on the limiting speed of drilling. However, the overall effect of machining force on the process is limited [3, 11].

**Feed Rate:** If a constant velocity drilling method is used, the feed rate of the tool can be used as an actuator. The feed rate can influence the shape of the hole [7].

**Tool Vibration Properties:** Vibration can be added to the movement of the tool electrode in either constant velocity or gravity feed drilling methods. The parameters of this vibration (amplitude, frequency, duty cycle, etc.) can be modified on the fly and used as actuator signals. Tool vibration affects the speed of drilling. Amplitude of vibration is important in the machining speed, but frequency does not seem to have any effect [19].

**Tool Rotation Properties:** The speed of rotation for a rotating tool electrode is known to affect the hole shape as well as the drilling speed [21].

#### *4.2.2.3 Electrolyte Signals*

**Bulk Electrolyte Properties:** Modifying the bulk electrolyte properties, such as concentration, temperature, and level, would require the design of a new type of machining cell. The speed with which these parameters could be modified would be slower than, for example, the speed with which voltage can be modified. However, if the machining cell is sufficiently small, they could potentially be modified on a comparable time scale to the speed of the process. The electrolyte bulk properties are known to have an effect on several parameters of machining [1, 13, 14].

### 4.2.3 Selection of Signals

None of these signals have been previously used to implement a feedback controller. Using the combination of depth as a sensor signal and voltage as an actuator signal is one pair that makes sense. Voltage affects the speed of the process, or more precisely the depth evolution. Measuring the depth allows observation of the affect voltage has on the depth evolution directly. It is this pair which is examined in this chapter.

## 4.3 Position feedback controllers

There are two feedback controllers considered in this section. Both controllers aim at reducing the variability of the drilling process. The steady state value of the coefficient of variation will be used as an indicator to judge the performance of the controllers.

### 4.3.1 Proportional Controller

#### *4.3.1.1 Formulation*

The first controller to be suggested in this thesis is a proportional feedback controller. A block diagram is shown in figure 4-1.

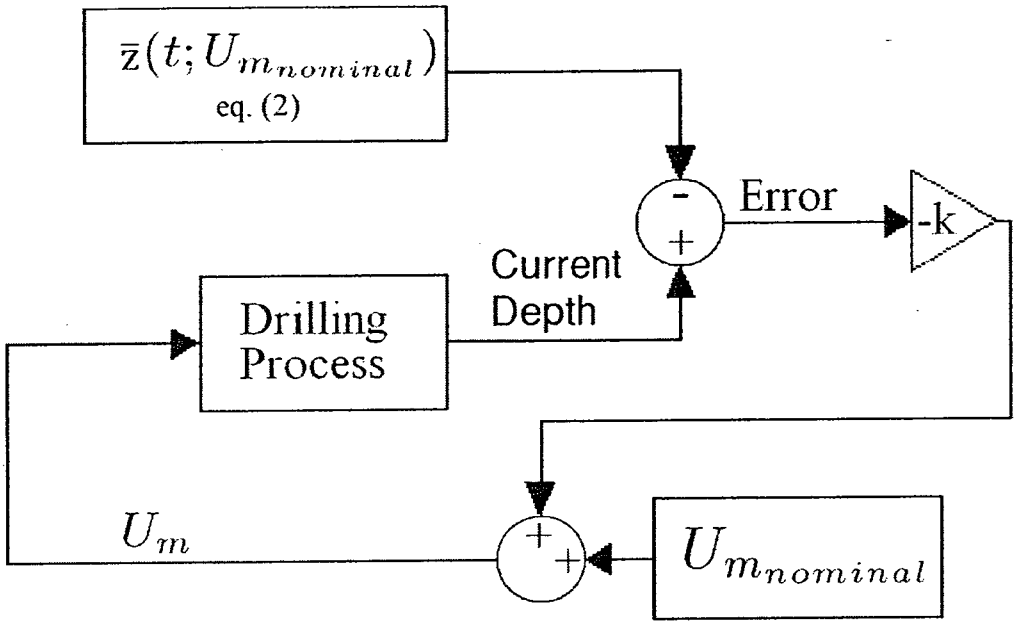


*Figure 4-1: Block diagram of first controller.*

The controller aims at forcing the drilling evolution to follow the natural mean evolution predicted by (2.9). The machining voltage $U_{machining}$ is set as

$$\begin{aligned} e &= z - \bar{z}(t; U_{m,nominal}) \\ U_m &= -k \times e + U_{m,nominal} \end{aligned}, \tag{4.1}$$

where $z$ is the current position of the tool, $k$ is the gain of the controller, and $U_{m,nominal}$ is the nominal voltage for the desired path. Furthermore, $U_m$ is restricted to the range of (28, 32) V. All of the gains used experimentally are selected using the following formula

$$k = \frac{2}{a \cdot \max_t(s(t))}, \tag{4.2}$$

where s(t) is sample standard deviation for the open loop experiment, and $a$ is the gain selecting parameter. The value of 2 found in the numerator correspond to half the size of the range of allowed voltages(i.e. 28 to 32 V). Selecting the gain with this equation ensures that the when the absolute value of the error is close to the maximum open loop sample standard deviation, the output voltage will be either 28 or 32 V. How close to the maximum open loop standard deviation depends on the value of the gain selecting parameter, which is varied to see the effect of the gain. However, it should be on the order of magnitude of one (i.e. a range of approximately 0.1-10). Values of $a$ that are very large would result in very minimal controller action, while values that are very small would result the applied voltage switching between just 28 and 32 V.

#### *4.3.1.2 Experimental Results*

Using this controller resulted in a significant decrease in the coefficient of variation in both the standard case and in the case where electrolyte level control and preheating is used (Figure 4-2). The coefficient of variation for the standard case was reduced by approximately a factor of three, while for the electrolyte level control and preheating case the reduction was only by a factor of two. The reason for the decrease in coefficient of variation can be attributed to the efforts of the controller to "push" the depth evolution toward the standard mean curve.

This fact leads to another interesting feature of the graph in Figure 4-2: there is not much difference, in terms of coefficient of variation, between the controller applied to the standard process and the controller applied to the process with electrolyte level control

and preheating. From a practical point of view, this is a very interesting result. It shows that the designed controller can be used to compensate for electrolyte bulk temperature and electrolyte level variations.

The fact that the controller obtains a similar steady state coefficient of variation in both the case with and without electrolyte level control and preheating requires some explanation. A plausible reason is that the controller can compensate for both the hole to hole transient elements, as well as other sources of variability. In the standard case the controller does both. In the other case there is no transient to remove and it just decreases the other sources of variation.

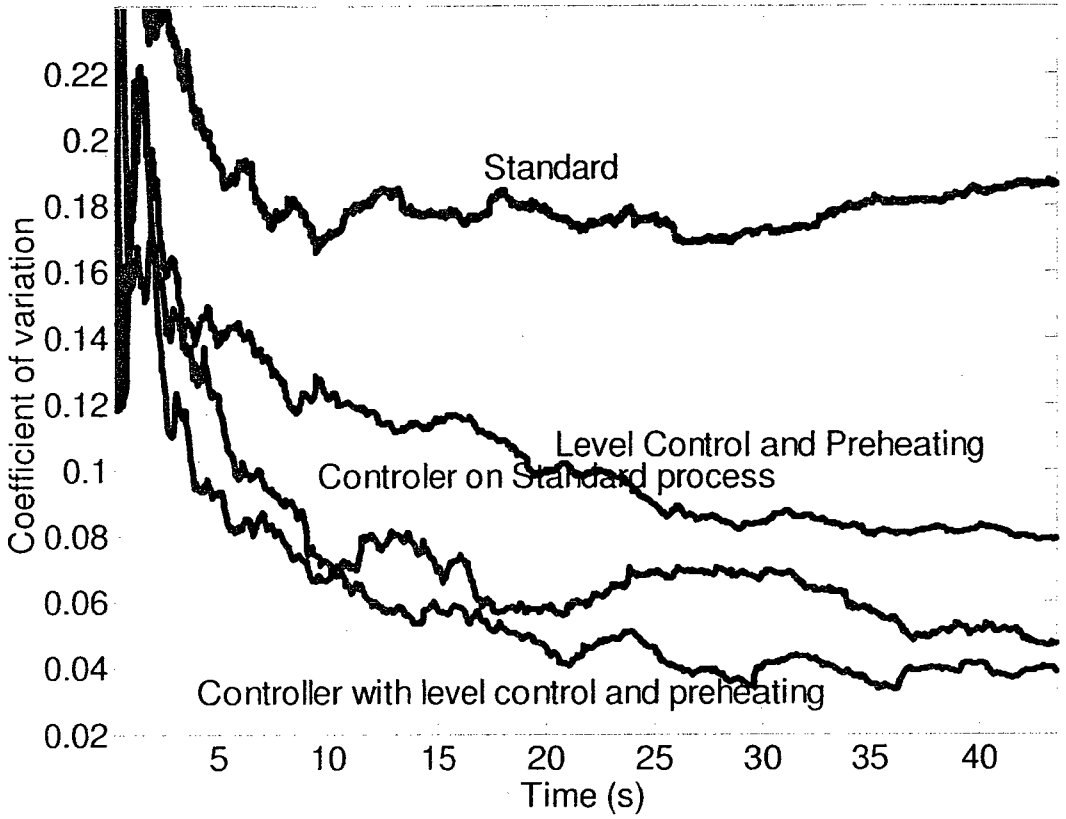


*Figure 4-2: Coefficient of variation for first controller machining with 0.04 v/um gain (corresponds to a=1). Data is shown for experiments with and without electrolyte preheating and level control, and for the first controller acting on the process with and without electrolyte preheating and level control. Note that a similar coefficient of variation is achieved by the controller regardless of whether there is electrolyte level control and preheating.*

#### *4.3.1.3 Agreement with Model*

The experimental results obtained with the controller are compared to the predictions of the model from chapter 2. Figure 4-3 shows the F-Statistics comparing the controller applied to the model in simulation, with a gain of 0.008 V/μm, and a nominal voltage of 30, to an experiment with the same parameters. From this graph of the F-Statistics, it can be concluded that there is insufficient evidence that the results of the model and the experiment differ significantly, except for a short time near the start of drilling. This is

similar to the agreement as seen in the constant voltage open loop example in chapter 2, which is a very encouraging sign for the validity of the model.

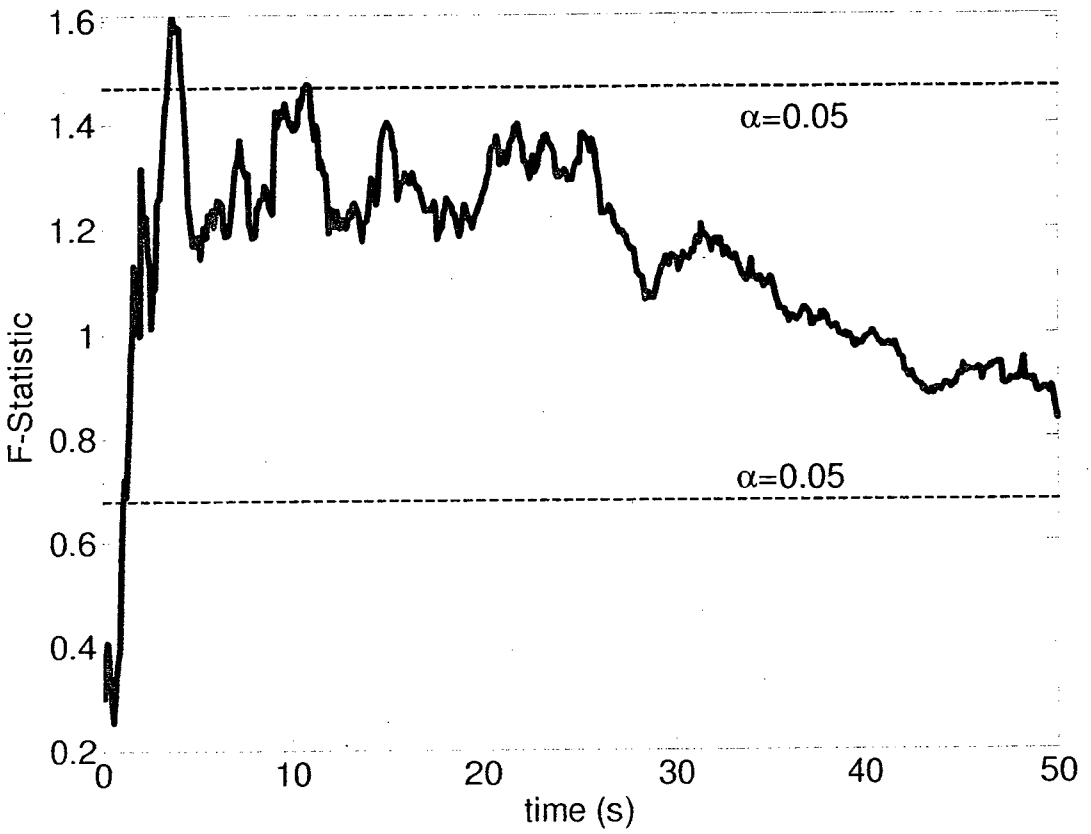


*Figure 4-3: F-Statistics plot for position controller with nominal voltage of 30 V and gain of 0.008V/μm (corresponds to a=0.2). The dashed lines show the critical range for a level of significance of 0.05.*

Figure 4-4 shows the F-Statistics for an experiment using a controller with a gain of 0.2 V/μm, a gain 25 times higher than the previous case examined of 0.008 V/μm. The F-Statistics shows enough evidence to reject the hypothesis that the variation of the model and the experiment are the same for over half of the time shown.

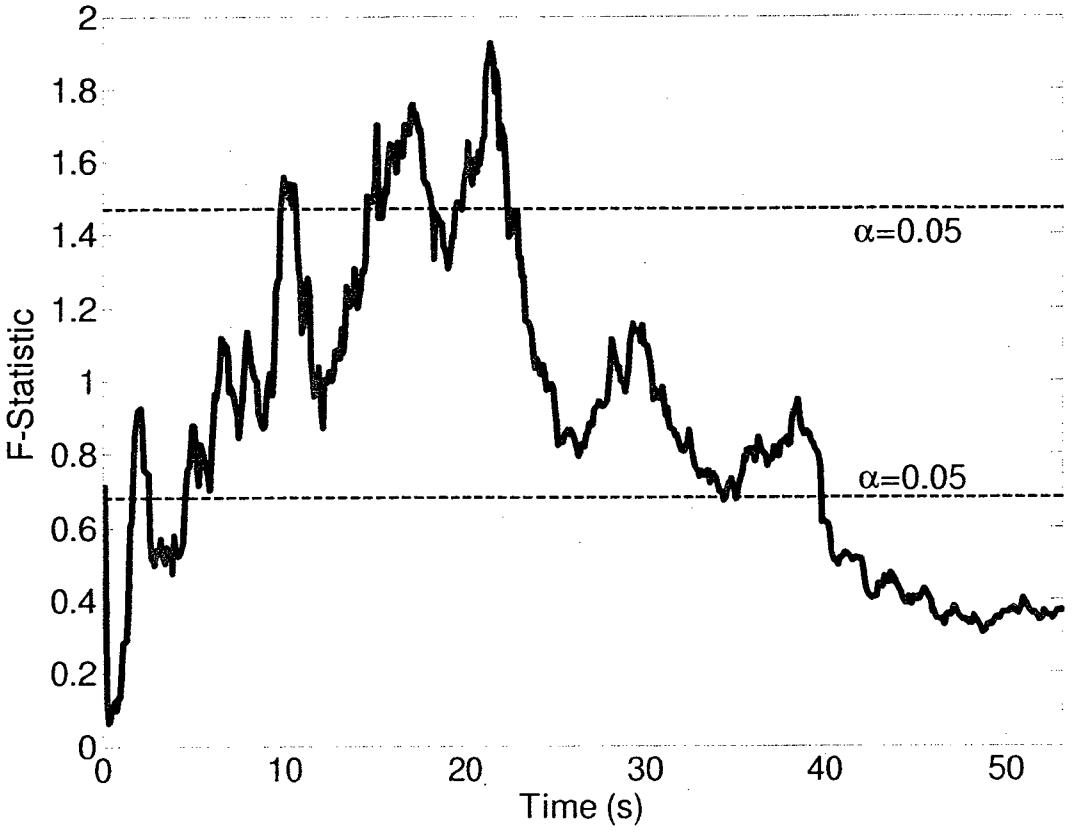


*Figure 4-4: F-Statistic plot for position controller with nominal voltage of 30 V and gain of 0.2V/μm (corresponds to a=5). The dashed lines show the critical range for a level of significance of 0.05.*

This is the first case where the model has failed to statistically agree with the experiment for such a large portion of the experiment. This can be explained by the fact that the changes in machining voltage made by the controller with a gain of 0.2 V/μm are faster than the voltage used in previous experiments examined in this thesis. Figure 4-5 shows a plot of the mean speed of change of the machining voltage (where speed of change is absolute value of rate of change) shows just how much faster the 0.2 V/μm gain experiment is compared to the 0.008 V/μm gain experiment. The average speed of change of voltage for the 0.008 V/μm gain experment is 5 V/s, while it is approximately 20 V/s

for the 0.2 V/μm gain. It is reasonable to conclude that the model is not accurate for fast changes in machining voltage. More specifically, for the case of experiments where the machining voltage is constantly changing (like the experiments discussed here), the model will work for an average speed of change of less than 5V/s, but not for greater than 20V/s.

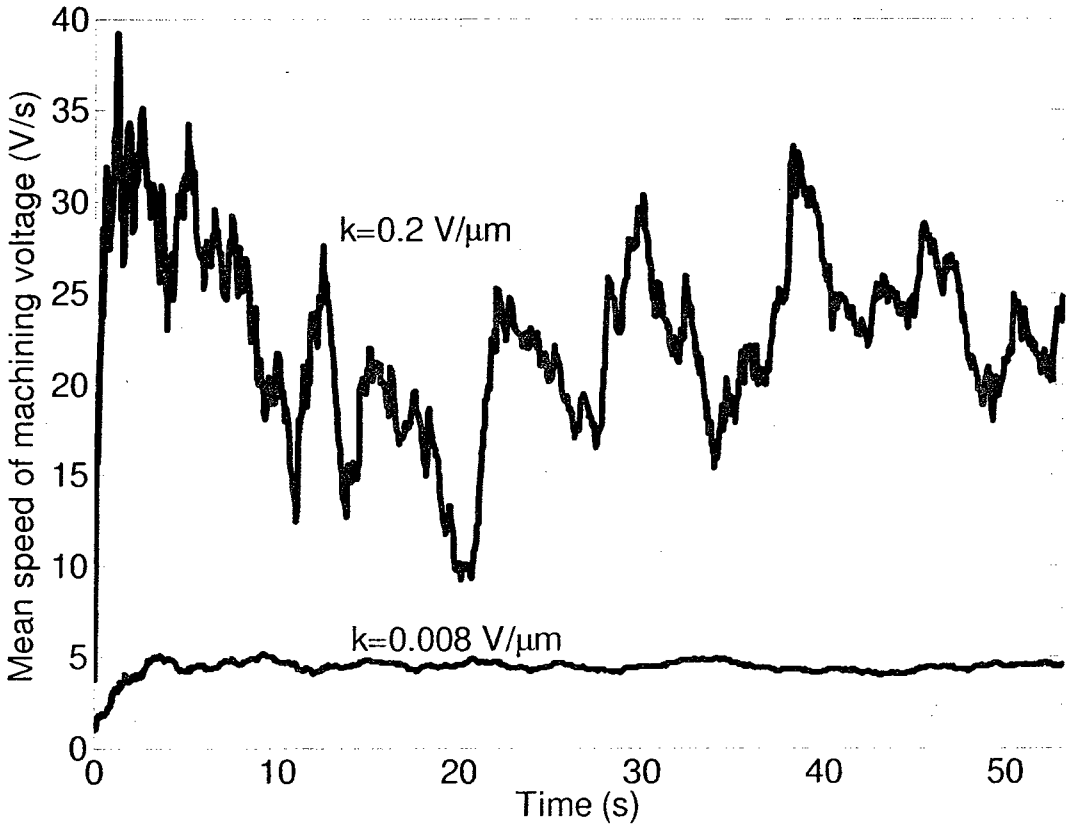


*Figure 4-5: Speed of change of the voltage for the k=0.2 V/μm experiment and the k=0.008 V/μm experiment. In general the k=0.2 V/μm has significantly faster changing voltage, usually well above 20 V/s, while the lower gain controller has a very consistent average speed of voltage at 5 V/s.*

It is also useful to note that model does have an accurate qualitative prediction, even for quickly changing machining voltages. The model predicts that the gain of 0.2 V/μm will

reduce the variation more than a gain of 0.008 V/μm does. This qualitative prediction holds true in practice. The experiment with 0.2 V/μm produces a steady state coefficient of variation of 0.03 while the 0.008 V/μm only get 0.07.

### 4.3.2 Smooth Zone Controller

#### *4.3.2.1 Formulation*

The second feedback controller to be proposed in this thesis sets the voltage as a function of the depth directly, as opposed to setting the voltage from some error value. The controller decreases the machining voltage as depth increases. The machining voltage is set through the equation

$$U_m(z) = (U_{max} - U_{min}) \cdot e^{-\lambda_{dec} \cdot z} + U_{min}, \tag{4.3}$$

where $U_{min}$, $U_{max}$, and $\lambda_{dec}$ are parameters of the controller. For example, the curve seen in figure 4-6, overlaid on the quality zone graph from figure 1-5 [16].

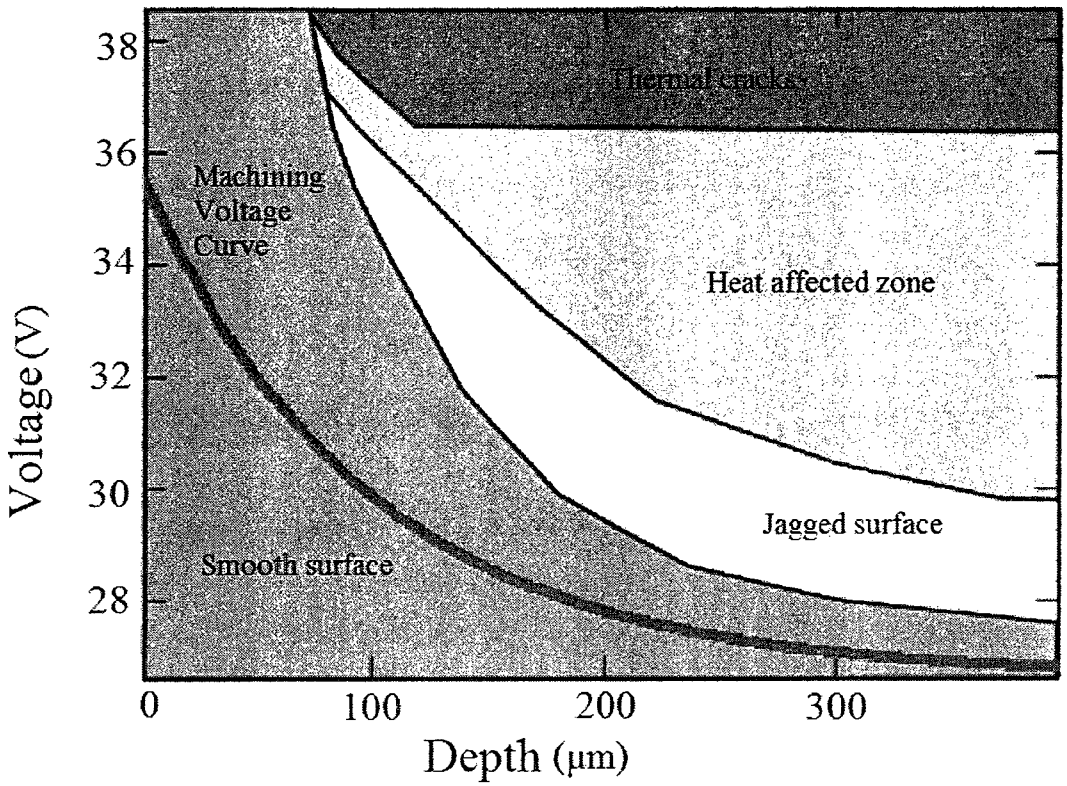


*Figure 4-6: A sample machining voltage curve for the second controller. The curve is overlaid on the depth-voltage quality zone plot from* [16]. *The curve's parameters are selected so that it stays in the "smooth surface" zone.*

The machining voltage curve in figure 4-6 uses the parameters $U_{min} = 26.5$, $U_{max} = 35$, and $\lambda_{dec} = 0.01$. These parameters were selected to ensure that the voltage will always stay within the "smooth surface" zone (see figure 4-6, the depth voltage-curve these values correspond is displayed). The parameters are selected in the order $U_{max}$, then $U_{diff}$, then finally $\lambda_{dec}$. Selecting the parameters is done according to the following guidelines:

- $\boldsymbol{U_{max}}$ will correspond to the initial value of the voltage, from figure 4-6 it appears that it can be selected to be any value as all initial voltages are within the smooth

surface zone. However, from the authors experience, too of a high value will cause damage to the work piece immediately after the voltage is switched on. Too low a value and the behaviour will be not much different than a constant voltage experiment. A range of between 32 and 36 volts will satisfy these guidelines.

- $U_{min}$ is the limiting voltage as the depth becomes large, it needs to be selected between the lowest voltage that will machine glass at all (around 26 V according to the authors experience) and the top of the smooth surface zone(28 V).
- $\lambda_{dec}$ determines the rate at which the voltage goes between $U_{max}$ and $U_{min}$, the higher the value the faster the transition. The main restriction is that the curve cannot cross out of the smooth surface zone before the desired depth is reached, which limits how low the value can be. The voltage will not ever intersect with it if $\lambda_{dec}$ >0.008.

#### *4.3.2.2 Experimental Results*

The machining voltage curve in figure 4-6 was used in conjunction with a standard experimental set-up. Figure 4-7 shows that the resulting coefficient of variation is similar to what is obtained by the first controller on the standard set-up (They both reach a steady state coefficient of variation of approximately 0.06).

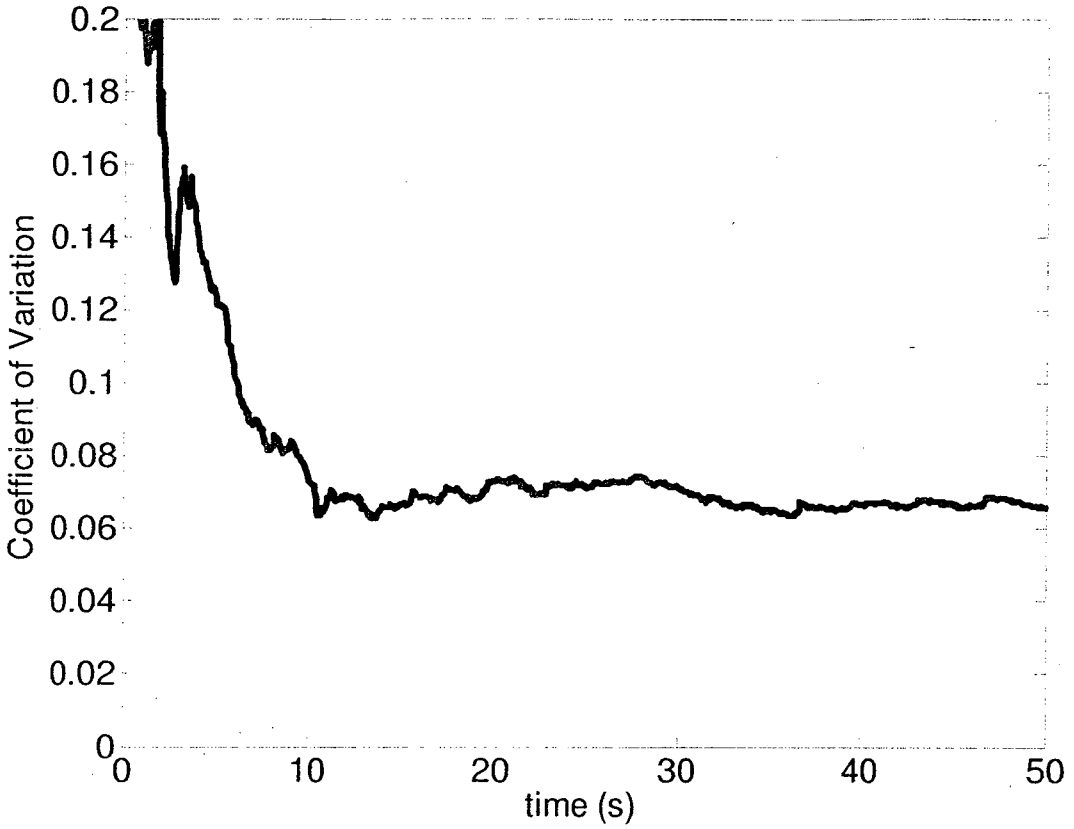


*Figure 4-7: The coefficient of Variation for the second controller. It obtains a similar coefficent of variation to the first controller.*

#### *4.3.2.3 Agreement with Model*

The F-Statistics for the experimental data and a simulation using the model from chapter 2 is shown in Figure 4-8. For a little under half the duration of the experiment the hypothesis that the model's variation matches the observed variation can be rejected with a 0.05 level of significance.

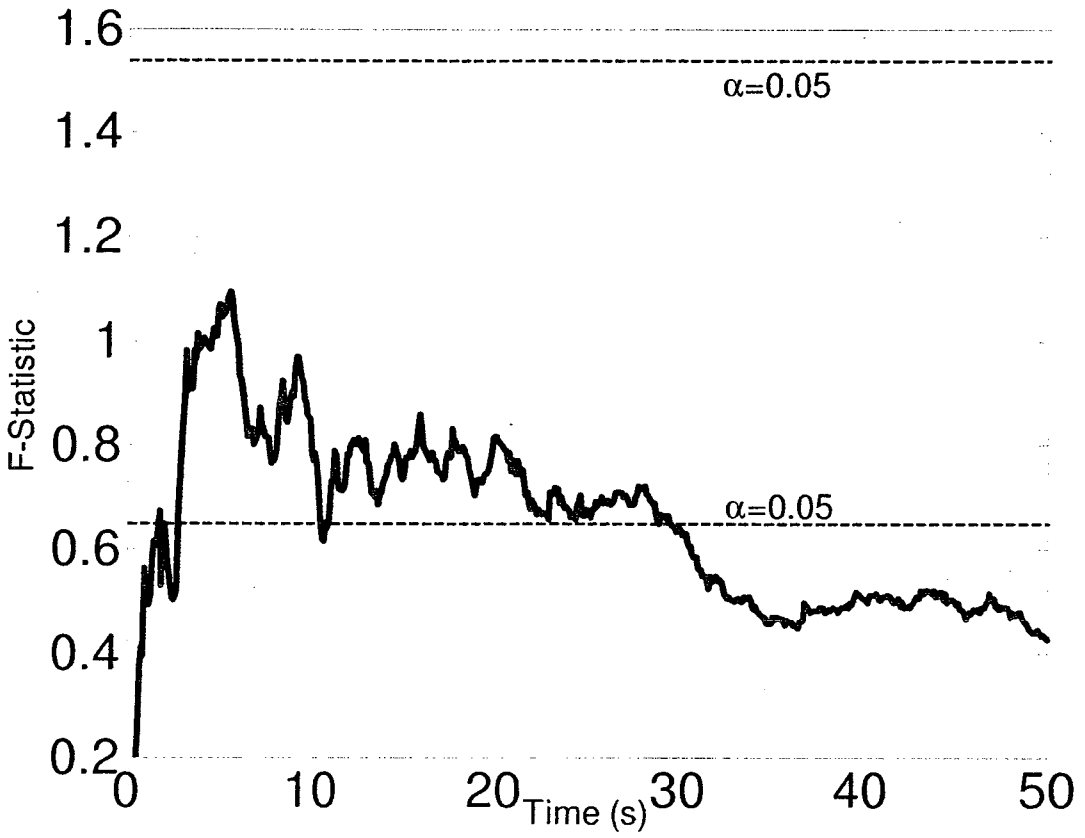


*Figure 4-8: F-Statistics for controller 2.*

The rate of change of the voltage in this experiment is very slow (near the beginning it is 6 V/s on average and decreases from then on), so this failure cannot be for the same reason as the high gain version of the first controller failed. Another feature that sets this experiment apart from others attempted is the range over which voltage changes; voltages between 35 and 27.5 V are applied. It is possible that the large range of values is causing the problems here. To test this an open loop experiment where the voltage is switched between 27 and 33 volts at 25 seconds is attempted. The F-statistics from this experiment

are seen in Figure 4-9. Clearly, the model fails in this case as well, indicating that the model does not accurately represent the system when a large change in voltage is made.

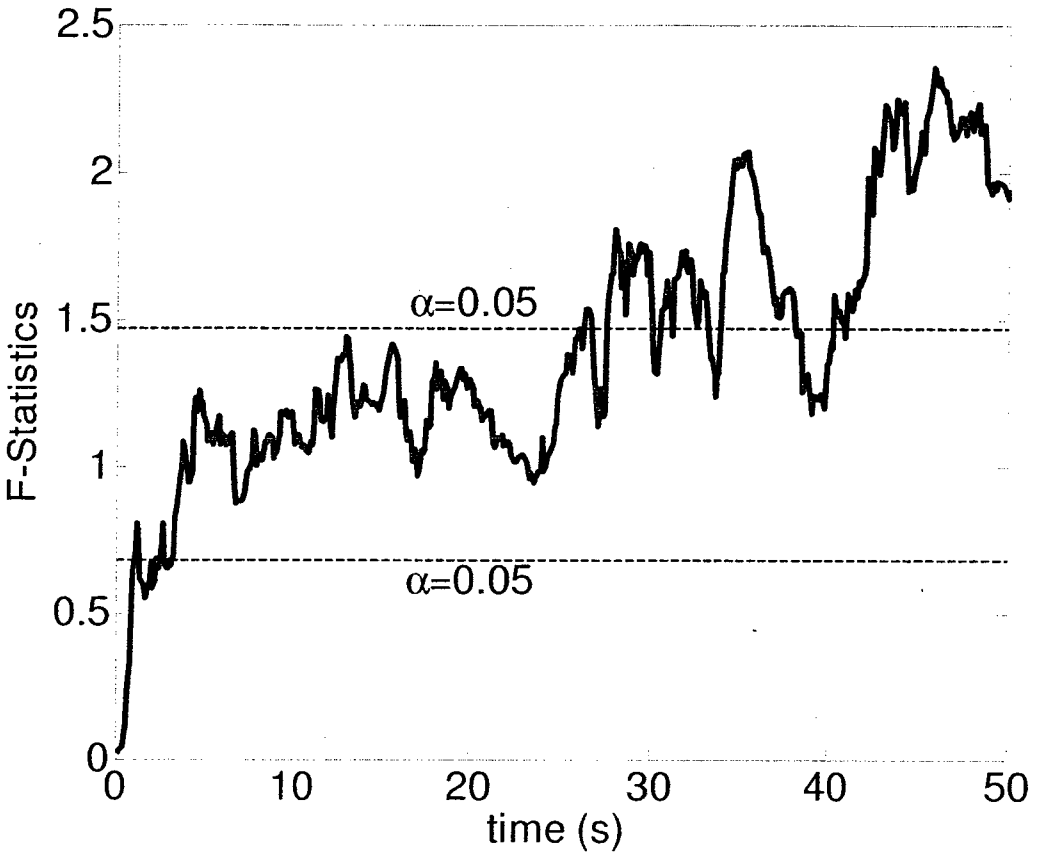


*Figure 4-9: F-Statistics for an experiment with a step increase in voltage from 27 to 33 volts at 25 seconds. The Dashed lines show the critical region for a level of significance of 0.05. After the step increase in voltage at 25 seconds, the F-Statistic passes above the α=0.05 line for most of the remained of the duration of the experiment.*

## 4.4 Summary

In this chapter the use of voltage as an actuator signal and machined depth as a sensor signal was motivated through a discussion of possible choices to add controllability and observability properties to the system. Experimental results for using these signals with

two different controllers were shown. In the first case the controller is seen to reduce the coefficient of variation of the SACE gravity drilling process by a factor of 3 when the standard set-up was used. The controller also reduces the variability when electrolyte level control and preheating are used, but only by a factor of 2. The second controller achieved a similar level of coefficient of variation as the first controller. These important results are summarized and compared to the most significant results from chapter 3 in table 4-2.

| Experiment | $c_v$ steady state value for standard process | $c_v$ steady state value for process with level control and preheating |
|---|---|---|
| Standard | 0.18±0.02 | 0.05±0.005 |
| First Controller | 0.06±0.01 | 0.04±0.005 |
| Second Controller | 0.06±0.01 | No Results |

*Table 4-2: Summary of steady state coefficient of variation results for controllers.*

The experimental results from both controllers were compared with the predictions made by simulation of the model from chapter 2. For the low gain experiment (k=0.008), the model predicts the results to within a 0.05 level of statistical significance for 90% of the duration of machining. However for higher gains the prediction only meets that level of significance for approximately 50% of machining duration. The poorer prediction for higher gains is thought to be because the model does not deal well with rapid changes in voltage (above 20V/s). Similarly, the results for the second controller are also not predicted well. The second controller varies voltage over a large range, so the poor

prediction in this case is added evidence that the model does not deal well with large changes in voltage, which is confirmed by secondary experiment. Both of these failures in the model can be a result of assumption 2 from 2.4.1.1 not holding true. That assumption is that $v_0$ and $\mu_0$ change instantaneously with voltage. Another possibility, also to do with assumption 2, is that $v_{lim}$, $\delta$ or $\sigma_j$ could be allowed to depend on voltage. Future work on the model should focus on adding dynamics to these parameters, or allowing other parameters to change with voltage.

# 5 Conclusion

## 5.1 Conclusions

- Two stochastic models were developed which are valid for both constant and time dependent voltage. The models were validated by showing that their predictions are within a statistical level of significance when compared to experimental data. The models accurately predict that the coefficient of variation always reaches a steady state value. Because it is a consistent feature, the steady state value of the coefficient of variation can be used to efficiently compare the variability between two sets of data.
- From examination of experimental evidence it was seen that
    - Preheating electrolyte to the temperature it generally reaches in steady state before an experiment begins reduces the steady state value of the coefficient of variation by a factor of two.
    - Controlling the electrolyte level to within ±0.05mm of a certain level could also reduce the steady state value of the coefficient of variation by a factor of two.
    - The combination of electrolyte preheating and electrolyte level control can reduce the steady state value of the coefficient of variation to 30 % of the standard value.
    - Tool vibration does not significantly affect variability, which is useful because it does increase the speed.

- It is possible to reduce the steady state value of the coefficient of variability by a factor of 3 from the standard case using feedback controllers, but neither electrolyte level control nor preheating can reduce it further.
- A limit on the validity of the developed model is seen. It was observed that the model is not valid for dealing with voltage changes at a rate higher than 20V/s nor for changes in voltage higher than 6 volts.

## 5.2 Future Work

Future work could include the following topics:

- Use the model developed to systematically evaluate the variability of other modifications to the SACE drilling process. e.g. tool rotation, voltage pulses, use of ultra-sonic wave in electrolyte etc.
- Modify the model to make it valid for higher rates of changes of voltage. One example would be to add dynamics to the velocity (as opposed to assuming it changes instantly with voltage changes).
- Develop a set-up which can precisely control the electrolyte properties; this would easily reduce the variability in the process by controlling them more exactly. Such a set-up would also be useful for further investigation on what effect these parameters have on drilling.
- Attempt to analyse the model and the controller formally. Such an analysis could show interesting information, e.g. what reduction variability would be expected for a certain gain. One route for analyses would be to follow the work of Hespanha [29]. The difference between the models analysed there and the models

developed here is that the rate of discrete evens is not polynomial here, the reset maps include a random value, and the process is unstable.

- Investigation of the link between variability in the depth evolution and variation in other elements of the hole (e.g. surface roughness or entrance diameter). This can be done more easily with the further understanding of variability in the depth evolution provided here.

## References


[1] R. Wüthrich, *Micromachining using Electrochemical Discharge Phenomenon Fundamentals and Applications of Spark Assisted Chemical Engraving.*William Andrew, 2009

[2] R. Wüthrich and V. Fascio, "Machining of non-conducting materials using electrochemical discharge phenomenon--an overview," *Int. J. Mach. Tools Manuf.,* vol. 45, *(9),* pp. 1095-1108, 2005.

[3] R. Wüthrich, U. Spaelter, Y. Wu and H. Bleuler, "A systematic characterization method for gravity-feed micro-hole drilling in glass with spark assisted chemical engraving (SACE)," *J Micromech Microengineering,* vol. 16, *(9),* pp. 1891-1896, 2006.

[4] Z. Zheng, W. Cheng, F. Huang and B. Yan, "3D microstructuring of Pyrex glass using the electrochemical discharge machining process," *J Micromech Microengineering,* vol. 17, *(5),* pp. 960-966, 2007.

[5] R. Wüthrich, K. Fujisaki, P. Couthy, L. A. Hof and H. Bleuler, "Spark assisted chemical engraving (SACE) in microfactory," *J Micromech Microengineering,* vol. 15, *(10),* pp. S276-S280, 2005.

[6] M. Esashi, Y. Matsumoto and S. Shoji, "Absolute pressure sensors by air-tight electrical feedthrough structure," *Sensors and Actuators A: Physical,* vol. 23, *(1-3),* pp. 1048-1052, 1990.

[7] E. S. Lee, D. Howard, E. Liang, S. D. Collins and R. L. Smith, "Removable tubing interconnects for glass-based micro-fluidic systems made using ECDM," *J Micromech Microengineering,* vol. 14, *(4),* pp. 535-541, 2004.

[8] J. West and A. Jadhav, "ECDM methods for fluidic interfacing through thin glass substrates and the formation of spherical microcavities," *J Micromech Microengineering,* vol. 17, *(2),* pp. 403-409, 2007.

[9] M. Han, B. Min and S. J. Lee, "Improvement of surface integrity of electro-chemical discharge machining process using powder-mixed electrolyte," *J. Mater. Process. Technol.,* vol. 191, *(1-3),* pp. 224-227, August 2007.

[10] H. Kurafuji and K. Suda, "Electrical discharge drilling of glass," *Annals of the CIRP,* vol. 16, pp. 415-419, 1968.

[11] M. Jalali, P. Maillard and R. Wüthrich, "Toward a better understanding of glass gravity-feed micro-hole drilling with electrochemical discharges," *J Micromech Microengineering,* vol. 19, *(4),* pp. 45001-45008, 2009.

[12] T. F. Didar, A. Dolatabadi and R. Wüthrich, "Local hardness and density variation in glass substrates machined with Spark Assisted Chemical Engraving (SACE)," *Materials Letters,* vol. 63, *(1),* pp. 51-53, Jan. 15. 2009.

[13] N. H. Cook, G. B. Foote, P. Jordan and B. N. Kalyani, "Experimental studies in electro-machining," *J Eng Ind Trans ASME,* vol. 96, pp. 945-950, 1973.

[14] C. T. Yang, S. S. Ho and B. H. Yan, "Micro Hole Machining of Borosilicate Glass trough Electrochemical Discharge machining (ECDM)," *Key Engineering Materials,* vol. 196, pp. 149-166, 2001.

[15] R. Wüthrich and L. A. Hof, "The gas film in spark assisted chemical engraving (SACE)—A key element for micro-machining applications," *International Journal of Machine Tools and Manufacture,* vol. 46, *(7-8),* pp. 828-835, 2006.

[16] P. Maillard, B. Despont, H. Bleuler and R. Wüthrich, "Geometrical characterization of micro-holes drilled in glass by gravity-feed with spark assisted chemical engraving (SACE)," *J Micromech Microengineering,* vol. 17, *(7),* pp. 1343-1349, 2007.

[17] R. Wüthrich, U. Spaelter and H. Bleuler, "The current signal in spark-assisted chemical engraving (SACE): what does it tell us?" *J Micromech Microengineering,* vol. 16, *(4),* pp. 779-785, 2006.

[18] A. Morrison, L. Rodrigues and R. Wüthrich, "Reducing variability in spark assisted chemical engraving gravity feed drilling of glass," 1st *Microsystems and Nanoelectronics Research Conference, 2008. MNRC 2008.* pp. 161-164, 2008.

[19] R. Wüthrich, B. Despont, P. Maillard and H. Bleuler, "Improving the material removal rate in spark-assisted chemical engraving (SACE) gravity-feed micro-hole drilling by tool vibration," *J Micromech Microengineering,* vol. 16, *(11),* pp. N28-N31, 2006.

[20] N. Gautam and V. K. Jain, "Experimental investigations into ECSD process using various tool kinematics," *Int. J. Mach. Tools Manuf.,* vol. 38, *(1-2),* pp. 15-27, 1998.

[21] Z. Zheng, H. Su, F. Huang and B. Yan, "The tool geometrical shape and pulse-off time of pulse voltage effects in a Pyrex glass electrochemical discharge microdrilling process," *J Micromech Microengineering,* vol. 17, *(2),* pp. 265-272, 2007.

[22] Z. Zheng, J. Lin, F. Huang and B. Yan, "Improving the machining efficiency in electrochemical discharge machining (ECDM) microhole drilling by offset pulse voltage," *J Micromech Microengineering,* vol. 18, *(2),* pp. 025014-025020, 2008.

[23] D. Kim, Y. Ahn, S. Lee and Y. Kim, "Voltage pulse frequency and duty ratio effects in an electrochemical discharge microdrilling process of Pyrex glass," *Int. J. Mach. Tools Manuf.,* vol. 46, *(10),* pp. 1064-1072, 2006.

[24] M. Han, B. Min and S. J. Lee, "Geometric improvement of electrochemical discharge micro-drilling using an ultrasonic-vibrated electrolyte," *J Micromech Microengineering,* vol. 19, *(6),* pp. 065004-065012, 2009.

[25] X. D. Cao, B. H. Kim and C. N. Chu, "Micro-structuring of glass with features less than 100 μm by electrochemical discharge machining," *Precis Eng,* vol. 33, *(4),* pp. 459-465, 10. 2009.

[26] V. K. Jain and S. Adhikary, "On the mechanism of material removal in electrochemical spark machining of quartz under different polarity conditions," *J. Mater. Process. Technol.,* vol. 200, *(1-3),* pp. 460-468, 2008.

[27] C. T. Yang, S. L. Song, B. H. Yan and F. Y. Huang, "Improving machining performance of wire electrochemical discharge machining by adding SiC abrasive to electrolyte," *Int. J. Mach. Tools Manuf.,* vol. 46, *(15),* pp. 2044-2050, 2006.

[28] R. E. Walpole, *Probability & Statistics for Engineers & Scientists.* ,8th ed.Upper Saddle River, NJ: Prentice Hall, 2007

[29] J. P. Hespanha, Modelling and analysis of stochastic hybrid systems. *Control Theory and Applications, IEE Proceedings; 153(5),* pp. 520-535, 2006.

[30] D. E. Knuth, *The Art of Computer Programming, Volume 2: Seminumerical Algorithms.* 3rd ed. Reading, Mass.; Upper Saddle River, NJ: Addison-Wesley, 1997; 2006

[31] A. Kulkarni, R. Sharan and G.K. Lal, "Measurement of temperature transients in the electrochemical discharge machining process," in Temperature: Its Measurement and Control in Science and Industry, 2003, pp. 1069-1074.

[32] A. Allagui and R. Wüthrich, "Gas film formation time and gas film life time during electrochemical discharge phenomenon," *Electrochim. Acta,* vol. 54, *(23),* pp. 5336-5343, 2009.

[33] R. Wuthrich, V. Fascio, D. Viquerat and H. Langen, "In situ measurement and micromachining of glass," *Proceedings of 1999 International Symposium on Micromechatronics and Human Science,* pp. 185-191, 1999.

[34] Nandkishor Dhawale. "Investigation of machining forces during constant velocity drilling in SACE (Spark Assisted Chemical Engraving) Technology" Masters Thesis, Concordia University, Montreal, 2009.